

























A hot Mars-sized exoplanet transiting an M dwarf

CALEB I. CAÑAS ^{1,2,*} SUVRATH MAHADEVAN ^{1,2} WILLIAM D. COCHRAN ³
CHAD F. BENDER ⁴ ERIC D. FEIGELSON ^{1,2} C. E. HARMAN ⁵ RAVI KUMAR KOPPARAPU ⁶
GABRIEL A. CACERES ⁷ SCOTT A. DIDDAMS ^{8,9} MICHAEL ENDL ³ ERIC B. FORD ^{1,10,2,11}
SAMUEL HALVERSON ¹² FRED HEARTY ^{1,2} SINCLAIRE JONES ¹³ SHUBHAM KANODIA ^{1,2}
ANDREA S.J. LIN ^{1,2} ANDREW J. METCALF ¹⁴ ANDREW MONSON ¹ JOE P. NINAN ^{1,2}
LAWRENCE W. RAMSEY ^{1,2} PAUL ROBERTSON ¹⁵ ARPITA ROY ^{16,17} CHRISTIAN SCHWAB ¹⁸
AND GUÐMUNDUR STEFÁNSSON ^{13,†}

¹*Department of Astronomy & Astrophysics, The Pennsylvania State University, 525 Davey Laboratory, University Park, PA 16802, USA*

²*Center for Exoplanets and Habitable Worlds, The Pennsylvania State University, 525 Davey Laboratory, University Park, PA 16802, USA*

³*Center for Planetary Systems Habitability and McDonald Observatory, The University of Texas at Austin, Austin, TX 78730, USA*

⁴*Steward Observatory, The University of Arizona, 933 N. Cherry Ave, Tucson, AZ 85721, USA*

⁵*NASA Ames Research Center, Moffett Field, CA 94035, USA*

⁶*Planetary Environments Laboratory, NASA Goddard Space Flight Center, Greenbelt, MD 20771, USA*

⁷*Teachers Pay Teachers, 111 East 18th St, New York, NY 10003, USA*

⁸*Time and Frequency Division, National Institute of Standards and Technology, 325 Broadway, Boulder, CO 80305, USA*

⁹*Department of Physics, University of Colorado, 2000 Colorado Avenue, Boulder, CO 80309, USA*

¹⁰*Institute for Computational & Data Sciences, The Pennsylvania State University, University Park, PA 16802, USA*

¹¹*Center for Astrostatistics, 525 Davey Lab, The Pennsylvania State University, University Park, PA 16802, USA*

¹²*Jet Propulsion Laboratory, California Institute of Technology, 4800 Oak Grove Drive, Pasadena, California 91109, USA*

¹³*Department of Astrophysical Sciences, Princeton University, 4 Ivy Lane, Princeton, NJ 08540, USA*

¹⁴*Space Vehicles Directorate, Air Force Research Laboratory, 3550 Aberdeen Ave SE, Kirtland AFB, NM 87117 USA*

¹⁵*Department of Physics & Astronomy, The University of California, Irvine, Irvine, CA 92697, USA*

¹⁶*Space Telescope Science Institute, 3700 San Martin Drive, Baltimore, MD 21218, USA*

¹⁷*Department of Physics and Astronomy, Johns Hopkins University, 3400 N Charles St, Baltimore, MD 21218, USA*

¹⁸*Department of Physics and Astronomy, Macquarie University, Balaclava Road, North Ryde, NSW 2109, Australia*

ABSTRACT

We validate the planetary nature of an ultra-short period planet orbiting the M dwarf KOI-4777. We use a combination of space-based photometry from Kepler, high-precision, near-infrared Doppler spectroscopy from the Habitable-zone Planet Finder, and adaptive optics imaging to characterize this system. KOI-4777.01 is a Mars-sized exoplanet ($R_p = 0.51 \pm 0.03R_\oplus$) orbiting the host star every 0.412-days (~ 9.9 -hours). This is the smallest validated ultra-short period planet known and we see no evidence

for additional massive companions using our HPF RVs. We constrain the upper 3σ mass to $M_p < 0.34 M_{\oplus}$ by assuming the planet is less dense than iron. Obtaining a mass measurement for KOI-4777.01 is beyond current instrumental capabilities.

Keywords: planets and satellites: detection — planetary systems — stars: fundamental parameters

1. INTRODUCTION

Ultra-short period planets (USPs) have orbital periods < 1 day and represent a rare class of exoplanet. A statistical study of the Kepler data (Sanchis-Ojeda et al. 2014) revealed 106 USP candidates and a dependence of the USP occurrence rate with the host star mass. Sanchis-Ojeda et al. (2014) calculated the occurrence rate of USPs to be $0.15 \pm 0.05\%$ for F dwarfs with a maximum occurrence rate of $1.10 \pm 0.40\%$ for M dwarfs. The Kepler (Borucki et al. 2010) and K2 (Howell et al. 2014) missions discovered only a few USPs transiting M dwarfs (e.g., Muirhead et al. 2012; Swift et al. 2013; Sanchis-Ojeda et al. 2015; Smith et al. 2018; Hirano et al. 2018). The first three years of the Transiting Exoplanet Survey Satellite (TESS; Ricker et al. 2015) have almost doubled the number of known USPs transiting M dwarfs with discoveries such as TOI-136 b (Vanderspek et al. 2019), TOI-732 b (Cloutier et al. 2020; Nowak et al. 2020), TOI-736 b (Crossfield et al. 2019), TOI-1078 b (Shporer et al. 2020), TOI-1634 b (Cloutier et al. 2021; Hirano et al. 2021), TOI-1635 b (Hirano et al. 2021), and TOI-1685 (Bluhm et al. 2021).

The formation mechanisms for USPs are not completely known, but many proposed formation scenarios invoke inward migration because the location of observed USPs is interior to the dust sublimation radius (Swift et al. 2013) and these regions would lack the materials necessary

for *in-situ* planet formation. Early formation scenarios proposed high-eccentricity migration in multi-planet systems (e.g., Schlaufman et al. 2010) where dynamical interactions with planets on wider orbits would excite the eccentricity of progenitor USP until tidal interactions with the host star become strong enough to decay the orbit. Other proposed scenarios include (i) low-eccentricity migration due to secular planet-planet interactions (Pu & Lai 2019), (ii) high-eccentricity migration due to chaotic secular interactions in compact multi-planet systems (Petrovich et al. 2019), (iii) tidal migration of USPs formed *in situ* in truncated planetary disks (Lee & Chiang 2017), (iv) obliquity-driven tidal migration (Millholland & Spalding 2020), and (v) migration of the outer planet in a resonant chain towards the inner edge of a gaseous protoplanetary disc due to gravitational instability (Zawadzki et al. 2021).

A majority of USPs are found in multi-planet systems (e.g., Sanchis-Ojeda et al. 2014; Adams et al. 2017; Winn et al. 2018) and, when observed in multi-planet systems, USPs have larger period ratios with their nearest neighbor when compared to the period ratios between neighboring planets of the same system (Steffen & Farr 2013; Winn et al. 2018), and larger mutual inclinations than when compared to planets on wider orbits (Dai et al. 2018). These observations suggest USPs have experienced inclination excitation and orbital shrinkage, which may indicate the existence of additional, non-transiting companions. USPs in multi-planet systems often have formation scenarios invoking perturbers, so radial velocity

* NASA Earth and Space Science Fellow

† Henry Norris Russell Fellow

(RV) or astrometric observations of such systems are important to place a constraint on additional, non-transiting planets. These well-characterized USP systems will be required to confirm and refine any USP formation scenarios.

In this paper, we investigate the M dwarf system, KOI-4777 ($V = 16.4$, $J = 13.2$), hosting a USP that was initially classified as a false positive by the Kepler DR25 automatic vetting. We validate the planetary nature of the Mars-sized ($R = 0.51 \pm 0.03 R_{\oplus}$) transiting companion. We use publicly available observations along with precision near-infrared (NIR) RVs with the Habitable-zone Planet Finder Spectrograph (HPF; Mahadevan et al. 2012, 2014) for statistical validation and to constrain the presence of non-transiting planets.

This paper is structured as follows. Section 2 presents the observations used in this paper and Section 3 describes the false positive analysis of KOI-4777.01 using the VESPA statistical validation tool (Morton 2012, 2015). Section 4 describes the method for spectroscopic characterization and our best estimates of the stellar parameters. In Section 5, we explain the analysis of the photometric and RV data while Section 6 provides further discussion of the bulk properties of the KOI-4777 system and the feasibility for future study through additional high-precision RV observations. Finally, we conclude the paper in Section 7 with a summary of our key results.

2. OBSERVATIONS

2.1. Photometry

Kepler observed KOI-4777 (KIC 6592335, Gaia EDR3 2102436351673656704) for the entirety of the original mission in long-cadence mode with data from 2009 May 13 through 2013 May 11. It is not included in the final catalog (DR25) released by the Kepler team, which uses a fully automated vetting pipeline (Cough-

lin et al. 2016; Mullally et al. 2016; Twicken et al. 2016) to catalog genuine transit events, or Kepler objects of interest (KOIs), in a uniform manner to maximize the reliability of the final catalog. The default search in the Kepler vetting pipeline did not consider transits with periods < 0.5 days (Coughlin 2019) and KOI-4777.01 was reported to have a period of 0.824 days, twice the true orbital period, and subsequently classified as a false positive. Manual vetting by members of the Kepler False Positive Working Group (FPWG) determined this system was a small planetary candidate with a period of 0.412 days. KOI-4777 is correctly identified in the supplemental Kepler DR25 candidate list as KOI-4777.01 (Thompson et al. 2018).

For our subsequent analysis, we used the entire pre-search data-conditioned (PDCSAP; Stumpe et al. 2012; Smith et al. 2012) light curves available at the Mikulski Archive for Space Telescopes (MAST). We use the PDCSAP light curves from all 17 quarters of Kepler and exclude observations with non-zero data quality flags. These flags indicate poor-quality data due to conditions such as spacecraft events or cosmic ray hits and are described in the Kepler Archive Manual (see Table 2-3 in Thompson et al. 2016). We do not perform additional processing or apply outlier rejection beyond the data quality flags. The raw photometry and the candidate signal are shown in Figure 1.

The true period was independently identified by Caceres et al. (2019a) in the application of the autoregressive planet search procedure (ARPS; Caceres et al. 2019b) to 156,717 Kepler PDCSAP light curves. The ARPS analysis has four stages: (i) fitting and removing non-stationary stellar variations with low-dimensional autoregressive integrated moving average (ARIMA) models, (ii) calculating a periodogram using the transit comb filter (TCF) for the residuals, (iii) classifying light curve and TCF features with a random forest classifier

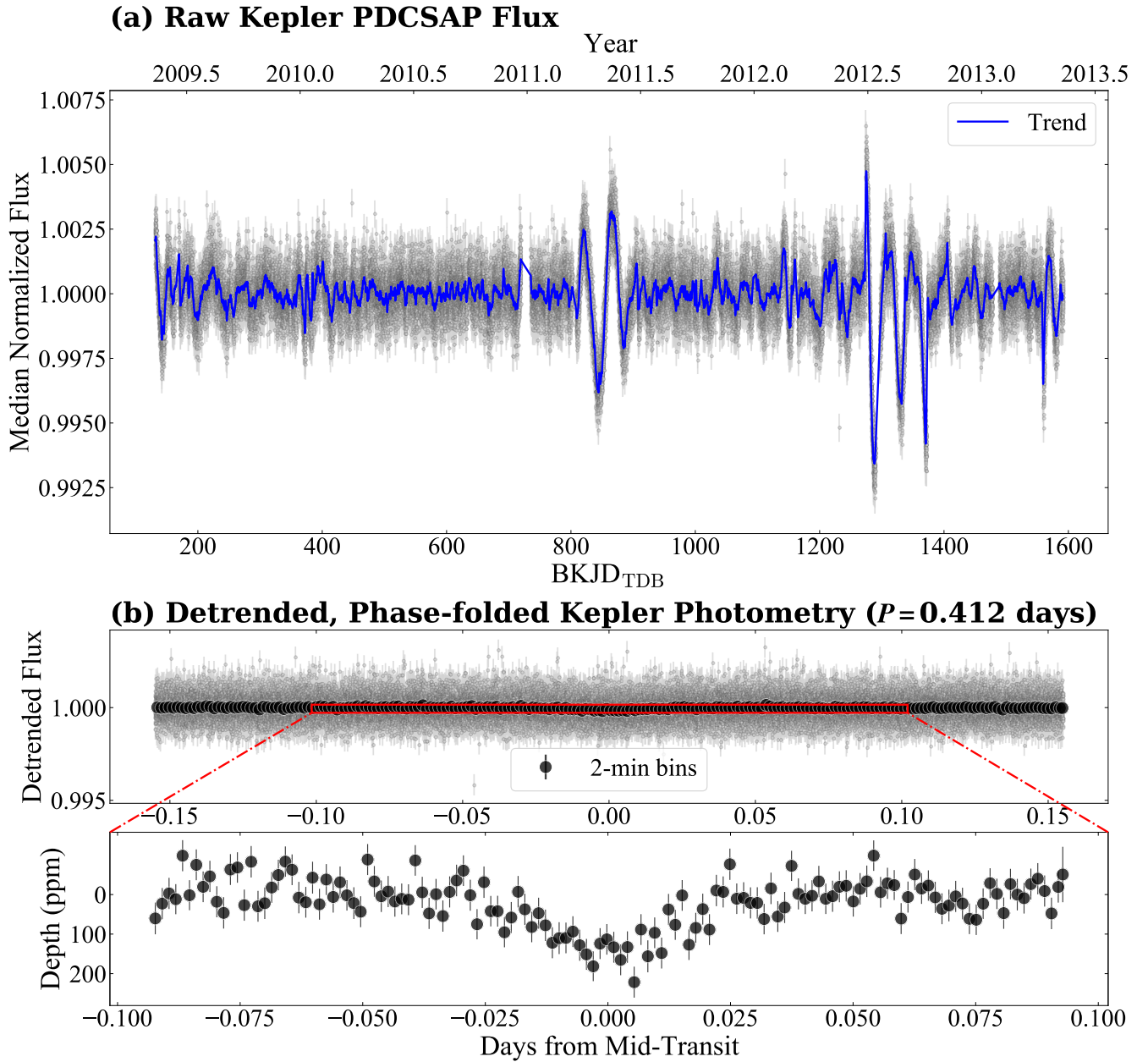


Figure 1. Kepler Photometry of KOI-4777. (a) displays the raw PDCSAP photometry from all 17 quarters of the Kepler mission. We have excluded observations with non-zero data quality flags. (b) shows the photometry after detrending with a Gaussian process and phasing to the observed ephemeris from the supplemental Kepler DR 25 catalog. In the bottom panel, we bin the phase-folded data into 2-min bins to show the shape of the transit.

trained on confirmed Kepler planet candidates, and (iv) vetting to remove false alarms and false positives. The fit removed nearly all of the variability seen in Figure 1(a).

The TCF periodogram of the residuals from the ARPS analysis for KOI-4777 is shown in Figure 2 and reveals a periodic signal at $P =$

0.412 days with $S/N=30$; weaker harmonics at 0.206 and 0.824 days are marked for reference. The transit depth estimated from the TCF matched filter is ~ 126 ppm with respect to the time-averaged median flux in the full Kepler light curve with an approximate transit duration of 0.5 hours. The random for-

est classifier, using several dozen features from different stages of the ARPS analysis, gives a high probability of planetary transit origin with $P_{RF} = 0.64$, considerably above the $P_{RF} = 0.35$ threshold chosen by [Caceres et al. \(2019a\)](#) to classify a transit as a planet candidate.

The detection of a 0.412-day transit-like periodicity in KOI-4777.01 is designated KACT 39 by [Caceres et al. \(2019a\)](#) in their list of 97 Kepler ARPS candidate planets. KOI-4777.01 has the second-highest random forest probability out of the 29 USP candidates. About 20 other KACT candidates have TCF spectral peaks with $\text{SNR} \geq 30$ with periods ranging from 0.2 to several days. KOI-4777.01 was also one of four objects where the DR25 KOI period was a long-period alias of the ARPS derived period, as the range of periods examined by the Kepler team excluded the true period.

2.2. High-resolution Doppler Spectroscopy

We obtained fifteen 945-second visits of KOI-4777 with HPF at a median signal-to-noise ratio (S/N) per 1D extracted pixel of 19 at 1000 nm. The HPF exposure time calculator¹ suggests a nominal observation of a star with the same J magnitude as KOI-4777 would have a median S/N per pixel of 25. HPF is a high-resolution ($R \sim 55,000$), NIR (8080 – 12780 Å) spectrograph located at the 10m Hobby-Eberly Telescope (HET) at McDonald Observatory in Texas ([Mahadevan et al. 2012, 2014](#)) that achieves a long-term temperature stability of ~ 1 mK ([Stefánsson et al. 2016](#)). Our observations span almost a year from 20 June 2019 through 31 July 2020 and were executed in a queue by the HET resident astronomers ([Shetrone et al. 2007](#)). We use the algorithms in the tool `HxRGproc` for bias noise removal, non-linearity correction, cosmic-ray correction, and slope/flux and variance image calculation ([Ni-](#)

[nan et al. 2018](#)) of the raw HPF data. The one dimensional spectra are reduced using the procedures in [Ninan et al. \(2018\)](#), [Kaplan et al. \(2019\)](#), and [Metcalf et al. \(2019\)](#).

HPF has a NIR laser frequency comb (LFC) calibrator to provide a precise wavelength solution and track instrumental drifts ([Metcalf et al. 2019](#)). We do not use simultaneous LFC calibrations during the observations to minimize the risk of contaminating our faint target spectrum with scattered light from the LFC and instead extrapolate the wavelength solution from LFC frames taken as part of standard evening/morning calibrations and from LFC calibration frames that are taken periodically throughout the night. The extrapolation from LFC frames enables precise wavelength calibration on the order of < 30 cm/s ([Stefánsson et al. 2020](#)), a value much smaller than the RV uncertainty for a faint target like KOI-4777.

The RVs are derived following the methodology described in [Stefánsson et al. \(2020\)](#). Briefly, we use a modified version of the `SpEctrum Radial Velocity AnaLyser` pipeline (`SERVAL`; [Zechmeister et al. 2018](#)), which employs the template-matching technique (e.g., [Anglada-Escudé & Butler 2012](#)) to derive RVs. `SERVAL` creates a master template from the observations and determines the Doppler shift for each individual spectrum by minimizing the χ^2 statistic. It generates the master template using all observed spectra for KOI-4777 after excluding regions with significant telluric contamination that are flagged with a synthetic telluric-line mask generated from `telfit` ([Gullikson et al. 2014](#)), a Python wrapper to the Line-by-Line Radiative Transfer Model package ([Clough et al. 2005](#)). `SERVAL` calculates the barycentric correction for each epoch using `barycorrpy` ([Kanodia & Wright 2018](#)), which uses the algorithms from [Wright & Eastman \(2014\)](#). Table 1 presents the de-

¹ <https://psuastro.github.io/HPF/Exposure-Times/#estimating-hpf-exposure-times>

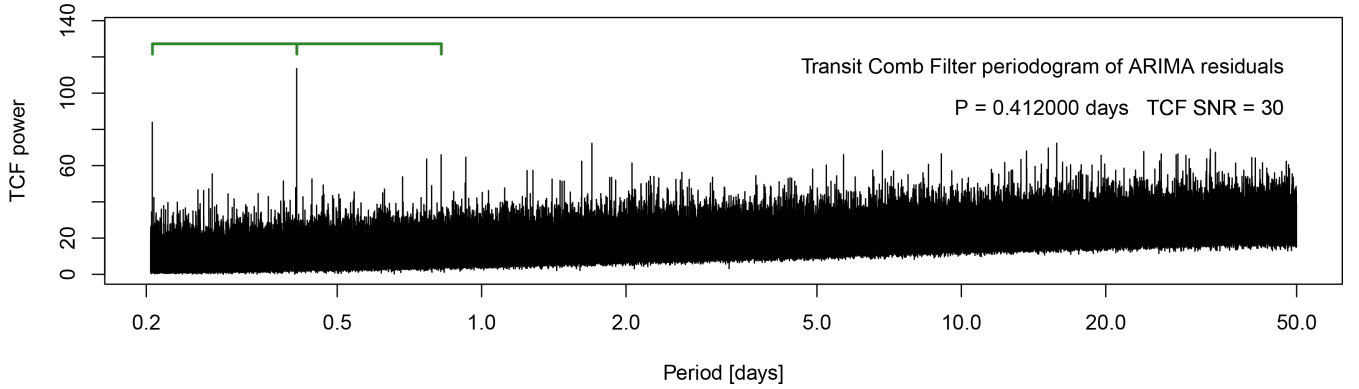


Figure 2. Detection of KOI-4777.01 with ARPS. The periodogram is displayed from 0.2 to 50 days of KOI-4777.01 (KIC 6592335) obtained with the transit comb filter method in the ARPS analysis of Kepler light curves (Caceres et al. 2019b,a). The strongest peak is at $P = 0.412$ days and its harmonics are marked in green.

Table 1. RVs of KOI-4777.^a

BJD _{TDB}	RV (m/s)	σ (m/s)	S/N ^b @1000 nm
2458654.956552	9	66	27
2458654.967588	213	92	27
2458656.941803	-68	131	19
2458656.953302	-120	103	19
2459004.772791	-28	140	16
2459004.783857	380	140	16
2459005.760007	-23	230	10
2459026.702878	21	152	18
2459026.714081	8	107	18
2459030.686671	-293	132	19
2459030.698159	61	100	19
2459045.652346	83	120	21
2459045.663519	29	93	21
2459061.845708	-10	85	23
2459061.857467	29	95	23

^aAll exposure times are 945s.

^bPer pixel

rived RVs, the 1σ uncertainties, and the S/N per pixel at 1000 nm for KOI-4777.

2.3. Sky-Projected Companions

To investigate the presence of background companions at separations $>4''$ from KOI-4777, we searched the entire region around KOI-4777 observed by Kepler using archival photometry and Gaia EDR3 (Gaia Collaboration et al. 2021). We use the Kepler target pixel files (TPFs; Kinemuchi et al. 2012) available on MAST to determine the extent of the sky contained in the Kepler footprint and obtain the optimal aperture used to generate the PDCSAP light curve. Figure 3 shows the TPF region for KOI-4777 and the respective apertures: the region of sky observed at least once by Kepler is indicated the dashed polygon while the region included in the optimal aperture masks is marked as a solid polygon.

Gaia EDR3 indicates that only KOI-4777 is contained in the Kepler footprint and in the optimal aperture. The region of sky around the Kepler footprint was observed by the first Palomar Sky Survey (POSS-I; Minkowski & Abell 1963) in 1951 and the Pan-STARRS1 Surveys (PS1; Chambers et al. 2016; Magnier et al. 2020) in 2011. Figure 3(a) presents the POSS-I red image overlaid with the Kepler footprint and aperture. KOI-4777 is off-center in the aperture and there are no additional bright background sources contained the aperture or footprint. Figure 3(b) displays the PS1 i image

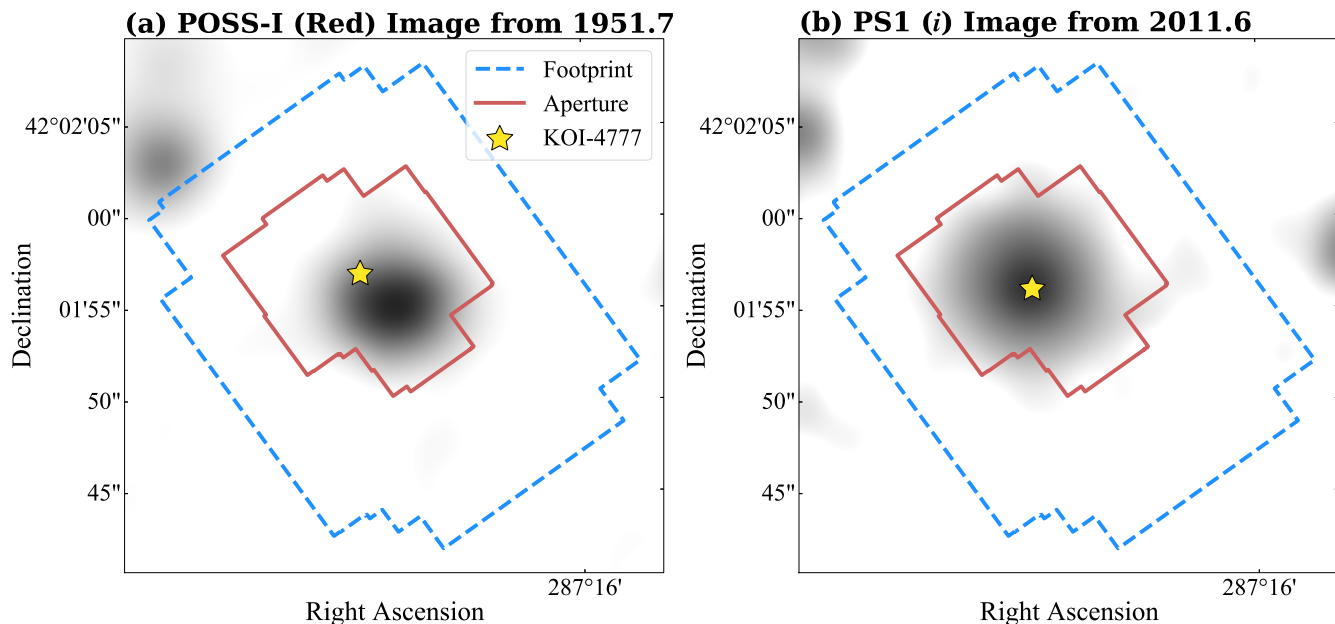


Figure 3. Stellar neighborhood around KOI-4777. **(a)** presents the cumulative Kepler footprint on a POSS-I red image from 1951. The blue dashed polygon is the region of the sky observed at least once in all seventeen quarters of the Kepler data. The red solid polygon is the cumulative region of sky contained at least once within the aperture pixel mask. KOI-4777 is marked as a star. Gaia EDR3 detects no bright $\Delta G < 4$ companions within the entire Kepler footprint. **(b)** is similar to Panel A but overlaid on a PS1 *i* image taken in 2011 when Kepler was observing this star. KOI-4777 has moved slightly but no other bright stars have moved into the aperture or Kepler footprint. When KOI-4777 was observed by Kepler, there were no bright stars in the aperture that could cause significant dilution.

of KOI-4777 with an identical overlay showing KOI-4777 is centered on the Kepler aperture and no other background stars have entered the Kepler footprint. KOI-4777 has no detectable bright on-sky companions in either Gaia EDR3 or archive imaging such that the Kepler light curve should not contain any significant dilution due to contaminating light from other stars.

2.4. High-Contrast Imaging

KOI-4777 was observed as part of the Robo-AO Kepler planetary candidate survey (Ziegler et al. 2018) on 19 June 2016. The observations were performed using the Robo-AO laser adaptive optics system (Baranec et al. 2013, 2014) on the 2.1-m telescope at Kitt Peak National Observatory (Jensen-Clem et al. 2018) using a 1.85-m circular aperture mask on the primary mirror. These observations were taken using a long-pass filter with a hard cut off at 600

nm that was designed by the Robo-AO team to approximate the Kepler bandpass at redder wavelengths and suppress blue wavelengths to minimize the impact on adaptive optics performance. The resulting 5σ contrast curve is shown in Figure 4. The Robo-AO observations reveal that are no bright ($\Delta\text{mag} < 4$) secondary companions within $4.0''$.

3. FALSE POSITIVE PROBABILITY ANALYSIS

The shallow depth reported by the Kepler DR25 supplemental catalog (121 ppm) prevents additional ground-based observations of a transit of KOI-4777.01. We instead employ the package Validation of Exoplanet Signals using a Probabilistic Algorithm (VESPA; Morton et al. 2016) to conduct a false-positive analysis of KOI-4777.01. The algorithm implements the statistical techniques described in Morton

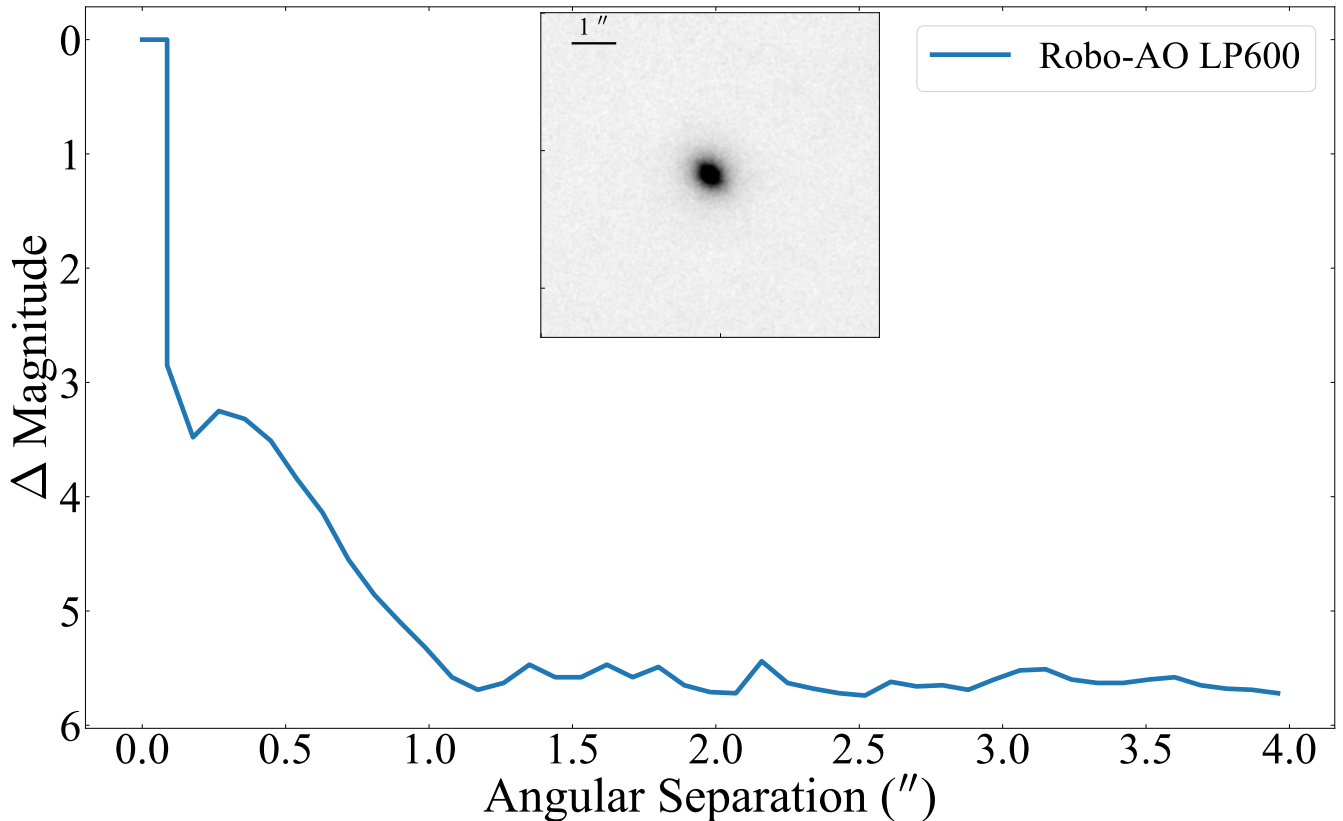


Figure 4. Robo-AO Imaging of KOI-4777. This figure displays the 5σ contrast curve observed by Ziegler et al. (2018) using Robo-AO in a long-pass filter with a hard cut off at 600 nm (LP-600). The data show there are no bright companions within $4''$ of the host star. The inset image is an $8''$ cutout centered on KOI-4777 in this long-pass filter. The contrast curve and image were obtained from the Robo-AO KOI survey (http://roboaokepler.org/koi_pages/KOI-4777.html).

(2012) to validate a planet by simulating and determining the likelihood of a range of astrophysical false-positive scenarios, including background eclipsing binaries (BEBs), eclipsing binaries (EBs), and hierarchical eclipsing binaries (HEBs). VESPA generates a population for each scenario and calculate the respective likelihood. KOI-4777.01 was previously analyzed by VESPA in Morton et al. (2016), albeit at twice the orbital period, where it was determined to have an FPP of 0.96 and most likely a background eclipsing binary.

We update the VESPA analysis with the period of $P = 0.412$ days (Coughlin 2019; Caceres et al. 2019b), and include the contrast curve from Robo-AO as an additional constraint to limit the brightness of any background compan-

ions within $4''$ of KOI-4777. As inputs to VESPA, we use the i) segment of the phase-folded Kepler transit centered on the transit and buffered by a baseline three times the transit duration, ii) 2MASS J , H , K and Kepler magnitudes, iii) Gaia EDR3 parallax, iv) host star stellar effective temperature, surface gravity, and metallicity. We set a uniform prior on the visual extinction where the upper limit is determined using estimates of Galactic dust extinction by Green et al. (2019). The maximum radius permissible for a BEB is the upper 3σ centroid offset determined by the Kepler DR 25 pipeline ($3.3169''$) and the maximum depth of the secondary transit is the rms of the light curve after excising the transits (< 190 ppm). We include the Robo-AO contrast curves shown in Figure 4 as a con-

straint applied to the BEB population during the VESPA analysis.

The shorter period used in this analysis meant that all EB systems at a period of 0.412 days would exceed the Roche limit of the host star (see Equation 2 in Eggleton 1983), such that the resulting system would be a contact or semi-detached binary and show a different morphology in the light curve than what is observed by Kepler. For our analysis, VESPA only considered the FPP contribution from double-period EB and HEB systems.

We obtain an FPP of 0.008 ± 0.001 for KOI-4777.01 from 100 bootstrap recalculations of the initially simulated populations for KOI-4777. Similar to the analysis by Morton et al. (2016), BEBs are the dominant FPP scenario and, adopting the threshold of 0.01 from Morton et al. (2016), KOI-4777 may be considered a validated planet.

4. STELLAR PARAMETERS

4.1. Spectroscopic Parameters

To derive spectroscopic stellar parameters of KOI-4777, we use HPF-SpecMatch (Stefánsson et al. 2020, Jones et. al. 2021 in prep) which is based on the methodology discussed in Yee

et al. (2017). HPF-SpecMatch derives the stellar properties of KOI-4777 by comparing the highest S/N HPF spectra of KOI-4777 to a library of 86 high quality ($S/N > 100$) HPF stellar spectra with well-determined properties (see Yee et al. 2017) spanning: $3000 \text{ K} < T_e < 5500 \text{ K}$, $4.4 < \log g < 5.2$, and $-0.5 < [\text{Fe}/\text{H}] < 0.5$.

For this analysis, HPF-SpecMatch compares the spectral order containing $8670 - 8750 \text{ \AA}$ to the HPF spectral library because there is minimal telluric contamination in the z -band. The algorithm identifies the best-matching library spectrum using χ^2 minimization, creates a composite spectrum from a weighted linear combination of the five best-matching library spectra, and derives the stellar properties using the calculated weights. The uncertainty for each stellar parameter (T_e , $\log g$, and $[\text{Fe}/\text{H}]$) is the standard deviation of the residuals from a leave-one-out cross-validation procedure applied to the entire stellar library in this wavelength region. The derived parameters for KOI-4777 are $T_{\text{eff}} = 3515 \pm 69 \text{ K}$, $[\text{Fe}/\text{H}] = 0.1 \pm 0.1$ and $\log(g) = 4.77 \pm 0.04$ and are listed in Table 2. KOI-4777 has an approximate M1.5 spectral type when using the T_e classification from Table 2 of Worthey (1994).

Table 2. Summary of Stellar Parameters.

Parameter	Description	Value	Reference
Main identifiers:			
KIC	...	6592335	KIC
KACT	...	39	ARPS
Gaia EDR3	...	2102436351673656704	Gaia EDR3
Equatorial Coordinates, Proper Motion, Distance, and Extinction:			
α_{J2016}	Right Ascension (RA)	19:09:02.92	Gaia EDR3
δ_{J2016}	Declination (Dec)	42:01:56.01	Gaia EDR3
l	Galactic Longitude	72.95336	Gaia EDR3
b	Galactic Latitude	14.74734	Gaia EDR3
μ_α	Proper motion (RA, mas/yr)	-2.149 ± 0.029	Gaia EDR3
μ_δ	Proper motion (Dec, mas/yr)	-13.853 ± 0.032	Gaia EDR3
d	Distance in pc ^a	$170.66^{+0.70}_{-0.74}$	Bailer-Jones

Table 2 continued

Table 2 (*continued*)

Parameter	Description	Value	Reference
$A_{V,max}$	Maximum visual extinction	0.03	Green
Optical and near-infrared magnitudes:			
B	Johnson B mag	18.305 ± 0.034	EHK
V	Johnson V mag	16.921 ± 0.022	EHK
J	2MASS J mag	13.221 ± 0.021	2MASS
H	2MASS H mag	12.671 ± 0.021	2MASS
K_s	2MASS K_s mag	12.449 ± 0.018	2MASS
$W1$	WISE1 mag	12.331 ± 0.023	WISE
$W2$	WISE2 mag	12.210 ± 0.022	WISE
$W3$	WISE3 mag	12.288 ± 0.274	WISE
Spectroscopic Parameters ^b :			
T_e	Effective temperature in K	3515 ± 69	This work
[Fe/H]	Metallicity in dex	0.1 ± 0.1	This work
$\log(g)$	Surface gravity in cgs units	4.77 ± 0.04	This work
Model-Dependent Stellar SED and Isochrone fit Parameters ^c :			
M_*	Mass in M_\odot	0.41 ± 0.02	This work
R_*	Radius in R_\odot	0.40 ± 0.01	This work
ρ_*	Density in g/cm^3	8.9 ± 0.6	This work
A_v	Visual extinction in mag	0.013 ± 0.009	This work
Other Stellar Parameters:			
$v \sin i_*$	Rotational velocity in km/s	< 2	This work
P_{rot}	Rotational period in days	44 ± 1	This work
Age	Age in Gyrs	$2 - 5$	This work
RV	Radial velocity in km/s	28.11 ± 0.05	This work
U, V, W	Barycentric Galactic velocities in km/s	$18.72 \pm 0.06, 23.46 \pm 0.05, 4.38 \pm 0.03$	This work
$U_{LSR}, V_{LSR}, W_{LSR}$	Galactic velocities w.r.t. LSR ^d in km/s	$29.8 \pm 0.8, 35.7 \pm 0.5, 11.6 \pm 0.4$	This work

References are: KIC (Brown et al. 2011), ARPS (Caceres et al. 2019b), Gaia EDR3 (Gaia Collaboration et al. 2021), Bailer-Jones (Bailer-Jones et al. 2021), Green (Green et al. 2019), EHK (Everett et al. 2012), 2MASS (Cutri et al. 2003), and WISE (Wright et al. 2010)

^a Geometric distance from Bailer-Jones et al. (2021).

^b Derived using our modified HPF-SpecMatch algorithm.

^c EXOFASTv2 derived values using MIST isochrones.

^d Calculated using the solar velocities from Schönrich et al. (2010).

We use `galpy` (Bovy 2015) to calculate the UVW velocities in the barycentric frame using the Gaia EDR3 proper motions and the systemic velocity derived from HPF. The reported values are in a right-handed coordinate system (Johnson & Soderblom 1987) such that UVW are positive in the directions of the Galactic center, Galactic rotation, and the north Galactic pole, respectively. The UVW velocities are

calculated with respect to the local standard of rest using the solar velocities and uncertainties from Schönrich et al. (2010). KOI-4777 is classified as a field star in the thin disk after applying the kinematic selection criteria from Bensby et al. (2014) to the derived UVW velocities. The BANYAN Σ algorithm (Gagné et al. 2018), which derives cluster membership probabilities using sky positions, proper motions, parallax, radial velocities, and spectrophotometric distance constraints, further classifies KOI-4777

as a field star that is not associated with any young clusters.

4.2. Spectral Energy Distribution Fitting

We use the EXOFASTv2 analysis package (Eastman et al. 2019) to model the spectral energy distribution (SED) and derive model-dependent stellar parameters using the MIST stellar models (Dotter 2016; Choi et al. 2016). EXOFASTv2 calculates the bolometric corrections for the SED fit by linearly interpolating the pre-computed bolometric corrections supplied by the MIST team in a grid of $\log g$, T_{eff} , $[\text{Fe}/\text{H}]$, and A_V^2 . The MIST grid is based on the ATLAS12/SYNTHÉ stellar atmospheres (Kurucz 1970, 1993). The fit uses Gaussian priors on the (i) 2MASS *JHK* magnitudes, Johnson *BV* magnitudes from Everett et al. (2012), and Wide-field Infrared Survey Explorer magnitudes (Wright et al. 2010); (ii) host star surface gravity, temperature, and metallicity derived with HPF-SpecMatch; and (iii) the geometric distance estimate from Bailer-Jones et al. (2021) and a uniform prior for the visual extinction in which the upper limit is determined from estimates of Galactic dust by Green et al. (2019) calculated at the distance determined by Bailer-Jones et al. (2021). The $R_v = 3.1$ reddening law from Fitzpatrick (1999) is used by EXOFASTv2 to convert the extinction determined by Green et al. (2019) to a visual magnitude extinction. The derived stellar parameters with their uncertainties are listed in Table 2. We derive a mass and radius of $0.41 \pm 0.02 M_{\odot}$ and $0.40 \pm 0.01 R_{\odot}$ for KOI-4777.

4.3. Rotation period & constraints on system age

The rotation period and kinematics for M dwarfs can provide an estimate of the age for the star because rapidly-rotating M dwarfs are typi-

cally younger than slowly-rotating counterparts (e.g., Irwin et al. 2011; Newton et al. 2016). Our analysis with HPF-SpecMatch also broadens the spectra using a linear limb darkening law (Yee et al. 2017) when generating the best-fitting template. Using our HPF spectra, we can only place a constraint of $v \sin i < 2 \text{ km/s}$ due to the resolution of $\sim 55,000$. The activity indicators from HPF spectra (see Zechmeister et al. 2018; Stefansson et al. 2020), including the differential line width, the chromatic RV index, and activity indices of the three lines in the Calcium II infrared triplet, show no variability and cannot be used to gauge the rotation period of the star. This suggests that KOI-4777 is probably not young and probably has a long rotation-period.

We use the available Kepler photometry to confirm the existence of a long rotation period. We do not search for a rotation period in the PDCSAP data (shown in 1) because the Kepler team warns that long period signals are attenuated in the PDCSAP flux and, in the latest iteration of the pipeline, the algorithm assumes all long period signals are systematics (see Section 5.15 in Van Cleve et al. 2016). Gilliland et al. (2015) showed that signals > 20 days are severely damped in the PDCSAP flux, although larger signals displayed comparatively better preservation at long periods. The Kepler team instead suggest searching for long-period signals by using the SAP flux and the available co-trending basis vectors (e.g., Aigrain et al. 2017; Cui et al. 2019).

For this work, we use the ARC2³ pipeline developed by Aigrain et al. (2017) to correct for systematics in the Kepler SAP light curve. The ARC2 pipeline performs the correction in two steps where it: (i) detects and removes isolated discontinuities from Kepler light curves (“jumps” in the data) and (ii) removes the in-

² http://waps.cfa.harvard.edu/MIST/model_grids.html#bolometric

³ <https://github.com/OxES/OxKeplerSC>

strument systematic trends from the photometry by using the publicly available co-trending basis vectors (CBVs; see [Kinemuchi et al. 2012](#)). [Aigrain et al. \(2017\)](#) note that the exact number of CBVs to use will vary, but the final correction is generally insensitive to the number of CBVs if more than 2-3 CBVs are used. To determine the number of CBVs to use for KOI-4777, we ran the ARC2 pipeline with anywhere from 2-8 CBVs and compared the generalized Lomb-Scargle (GLS) periodogram ([Zechmeister & Kürster 2009](#)) between 1-100 days for each detrended light curve. Using seven CBVs provided the highest power in the periodogram, and we adopt this as our detrended SAP photometry. All light curves derived from ARC2 had a significant peak at ~ 43 days regardless of the number of CBVs used.

We apply three common methods of time series analysis (see [Canto Martins et al. 2020](#); [Reinhold & Hekker 2020](#)) to search for the rotation period in the detrended SAP flux: the GLS periodogram, the wavelet power spectrum (e.g., [Bravo et al. 2014](#)), and the auto-correlation function (ACF) (e.g., [McQuillan et al. 2013a,b](#)). All three methods indicate a rotation period in the range of 25-50 days, but the periods differ from each other due to the shape of the light curve and the non-uniformity of the sampling. To further constrain the rotation period, we employ the `juliet` analysis package ([Espinoza et al. 2019](#)) to model the SAP photometry using the `celerite` package and the approximate quasi-periodic covariance function from ([Foreman-Mackey et al. 2017](#)). This covariance function (Equation 56 in [Foreman-Mackey et al. 2017](#)) takes the form of

$$k(\tau) = \frac{B}{2+C} e^{-\tau/L} \left[\cos\left(\frac{2\pi\tau}{P_{\text{GP}}}\right) + (1+C) \right], \quad (1)$$

where τ is the scalar of choice (for KOI-4777, we use time), and B , C , L , and P_{GP} are the hyperparameters of the covariance function. B and C determine the weight of the exponential

term with a decay constant of L (in days). P_{GP} determines the periodicity of the quasi-periodic oscillations and is taken as an estimator of the stellar rotation period. Equation 1 has been shown to reproduce the behavior of a more traditional quasi-periodic covariance function and has allowed for computationally efficient inference of stellar rotation periods even for large datasets that are not uniformly sampled (e.g., [Angus et al. 2018](#)). We place a broad uniform prior on the rotation period of 1 – 100 days. `juliet` performs the parameter estimation using `dynesty` ([Speagle 2020](#)), a dynamic nested-sampling algorithm. Figure 5 displays the SAP photometry, the best fitting Gaussian process model, and the results from the GLS, wavelet transform, and the ACF.

The Gaussian process modeling indicates a rotation period of $P_{\text{rot}} = 44 \pm 1$ days. Our period estimate is consistent with the period of 44.61 ± 20.51 days determined by [McQuillan et al. \(2013a\)](#) using the first 4 quarters from Kepler. KOI-4777 has an intermediate rotation period using the classification criteria from [Newton et al. \(2016\)](#), who were able to show that M dwarfs with $P_{\text{rot}} < 10$ days have a mean age of 2 Gyr while those with $P_{\text{rot}} > 70$ days have mean ages of ~ 5 Gyr. There is no age range for M dwarfs with rotation periods spanning 10–70 days in [Newton et al. \(2016\)](#) because this regime was sparsely populated. With this measured rotation period, KOI-4777 may have an age between 2–5 Gyr. This range is compatible with our model-dependent SED fit and still allows for the existence of KOI-4777.01, as USPs have been shown to be stable against tidal inspiral during the lifetime of main sequence stars ([Hamer & Schlaufman 2020](#)).

5. TRANSIT AND RADIAL VELOCITY MODELING

We use `juliet` to jointly model the Kepler PDCSAP photometry and HPF RVs. `juliet` calculates the transit model with the `batman`

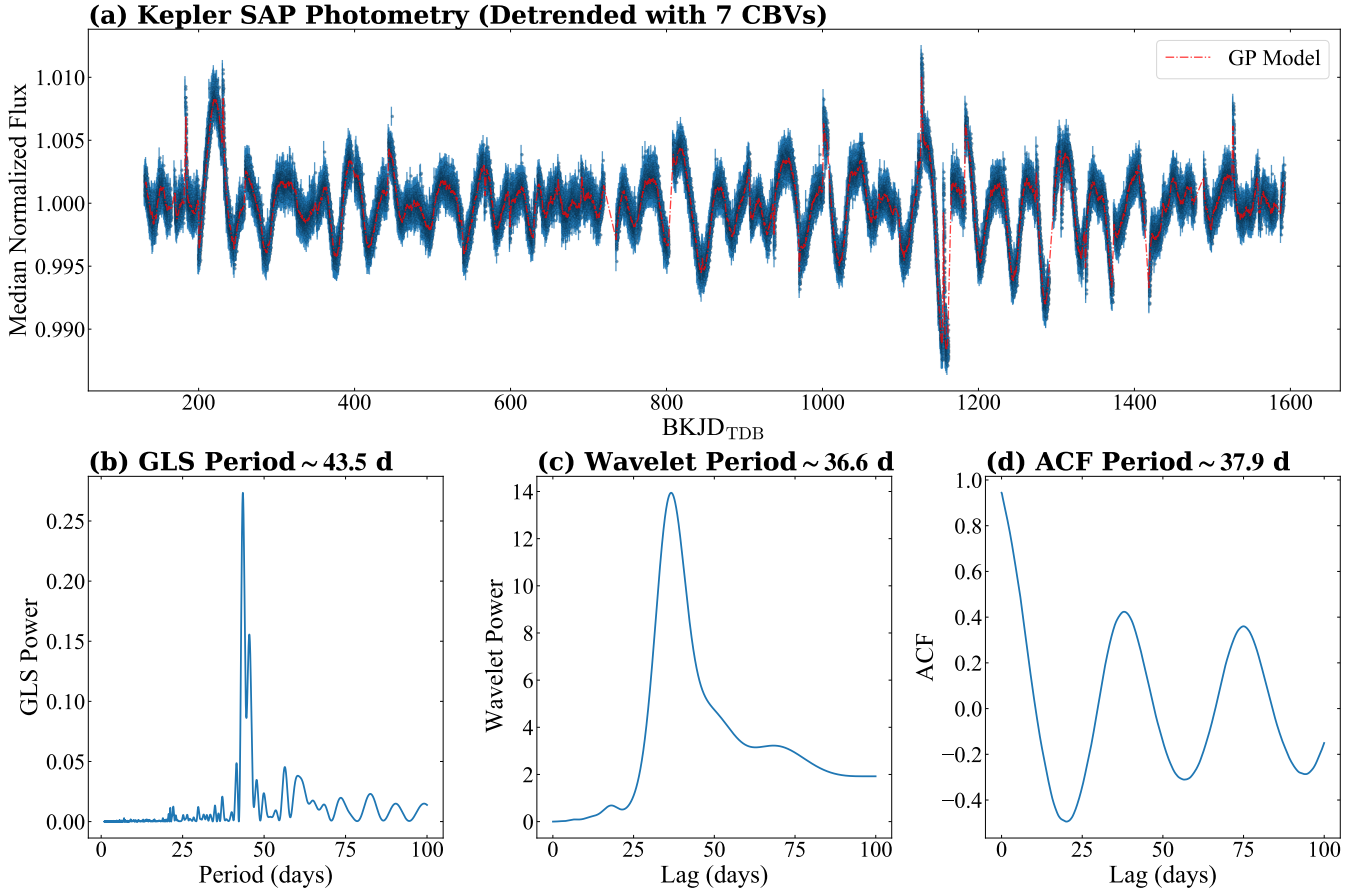


Figure 5. Rotation period of KOI-4777. (a) displays the median-normalized Kepler SAP photometry, after detrending with seven CBVs, along with our Gaussian process (GP) model as the dash-dotted line. (b) shows the generalized Lomb-Scargle (GLS) periodogram, (c) the time lags derived via wavelet decomposition, and (d) shows the autocorrelation function of the photometry in panel (a). Each method in panels (b) - (d) shows a significant peak between 25 - 50 days.

package (Kreidberg 2015) and uniformly samples the limb-darkening parameters using the parameterization from Kipping (2013a). The transit model utilizes the supersampling option in `batman` with exposure times of 30 minutes and a supersampling factor of 30 due to the long-cadence of the Kepler data. To account for correlated noise in the Kepler PDCSAP photometry, the fit includes a Gaussian process noise model identical to the one discussed in Section 4.3. `juliet` models the RVs with a standard Keplerian RV curve generated from the `radvel` (Fulton et al. 2018) package. Both the transit and RV models include a simple white-noise model in the form of a jitter term that is added in quadrature to the uncertain-

ties. We adopt a circular orbit and force an eccentricity of $e = 0$ because the circularization timescale (see Goldreich & Soter 1966; Jackson et al. 2008b) for KOI-4777.01 is $< 100,000$ years even if we conservatively adopt a tidal quality factor $Q_p = 500$ for a terrestrial planet (e.g., Jackson et al. 2008a) and a planetary mass of $1M_{\oplus}$. We also set a prior on the stellar density using the value determined from our EXOFASTv2 SED fit.

Figure 6 presents the results of the fit and Table 3 provides a summary of the derived system parameters and respective confidence intervals. The joint fit to the photometric and spectroscopic data indicate KOI-4777.01 is a Mars-sized transiting companion ($0.51 \pm 0.03 R_{\oplus}$) on

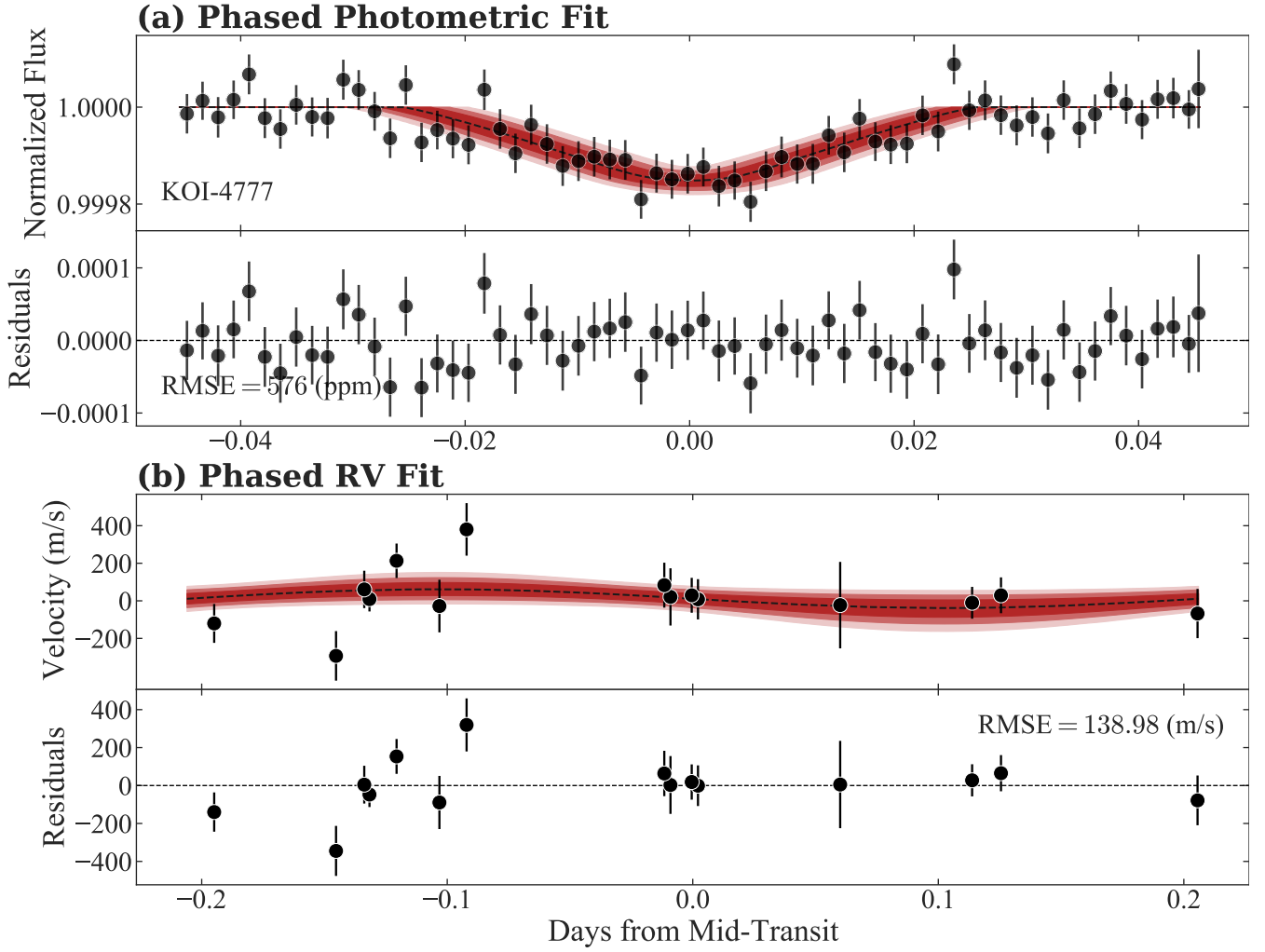


Figure 6. (a) displays the photometric model and the phased Kepler light curve. For clarity, we only show the phase-folded data after rebinning to 2-min bins (similar to Figure 1(b)). (b) presents the RVs after phasing the data to the ephemeris derived from the joint fit. For panels (a) and (b), the best-fitting model is plotted as a dashed line while the shaded regions denote the 1σ (darkest), 2σ , and 3σ range of the derived posterior solution.

a 0.412000 ± 0.000001 day orbit. These results are consistent to within their 1σ uncertainties to values obtained from EXOFASTv2 for a joint fit of the SED, HPF RVs, and the detrended photometry from the juliet fit. The HPF RVs place an upper mass constraint of $99.2M_{\oplus}$ at

the 99th quantile of the posterior distribution, which further strengthens the planetary validation because the observed transit cannot be due to an eclipsing stellar companion or a massive, grazing sub-stellar companion.

Table 3. Derived Parameters for KOI-4777

Parameter	Units	Prior	Value
Transit Parameters:			

Table 3 continued

Table 3 (*continued*)

Parameter	Units	Prior	Value
Linear Limb-darkening Coefficient ...	q_1	$\mathcal{U}(0, 1)^a$	$0.3^{+0.4}_{-0.2}$
Quadratic Limb-darkening Coefficient	q_2	$\mathcal{U}(0, 1)$	0.4 ± 0.3
Scaled Radius	R_p/R_*	$\mathcal{U}(0, 1)$	0.0116 ± 0.0006
Impact Parameter	b	$\mathcal{U}(0, 1)$	$0.2^{+0.2}_{-0.1}$
Photometric Jitter	σ_{Kepler} (ppm)	$\mathcal{J}(10^{-6}, 5000)^b$	165 ± 6
RV Parameters:			
Orbital Period	P (days)	$\mathcal{N}(0.412, 0.01)^c$	0.412000 ± 0.000001
Time of Conjunction	T_C (BJD _{TDB})	$\mathcal{N}(2454964.80421, 0.01)$	2454965.219 ± 0.002
Eccentricity	e	Fixed	0
Argument of Periastron	ω (degrees)	Fixed	90
Semi-amplitude Velocity	K (m/s)	$\mathcal{U}(0, 10^3)$	$3\sigma < 83$
RV zeropoint	γ_{HPF} (m/s)	$\mathcal{U}(-10^{-3}, 10^3)$	10 ± 30
RV jitter	σ_{HPF} (m/s)	$\mathcal{J}(10^{-3}, 10^3)$	$0.6^{+24.8}_{-0.6}$
Gaussian Process Hyperparameters:			
B	Amplitude (10^{-6} ppm)	$\mathcal{J}(10^{-6}, 1)$	$1.2^{+0.2}_{-0.1}$
C	Additive Factor (10^{-4})	$\mathcal{J}(10^{-6}, 10^6)$	0.000 ± 0.007
L	Length scale (days) ...	$\mathcal{J}(10^{-6}, 10^6)$	27^{+4}_{-3}
P_{GP}	Period (days)	$\mathcal{J}(1, 2000)$	37 ± 2
Derived Planetary Parameters:			
Scaled Semi-major Axis	a/R_*	4.28 ± 0.09
Orbital Inclination	i (degrees)	87 ± 2
Transit Duration	T_{14} (hours)	$0.73^{+0.02}_{-0.04}$
Mass	M_p (M_{\oplus})	$3\sigma < 99.2$
Radius	R_p (R_{\oplus})	0.51 ± 0.03
Semi-major Axis	a (au)	0.0080 ± 0.0003
Average Incident Flux	$\langle F \rangle$ (10^8 erg/s/cm ²)	4.4 ± 0.3
Equilibrium Temperature ^d	T_{eq} (K)	1180 ± 20

^a $\mathcal{U}(a, b)$ is a uniform distribution defined between lower limit a and upper limit b .

^b $\mathcal{J}(a, b)$ is a log-uniform distribution defined between lower limit a and upper limit b .

^c $\mathcal{N}(a, b)$ is a normal distribution with mean a and standard deviation b .

^dThe planet is assumed to be a black body.

6. DISCUSSION

6.1. Constraints on Long-period Companions

We use `thejoker` (Price-Whelan et al. 2017) to perform a rejection sampling analysis on the HPF RVs and place a constraint on the existence of long-period giant companions. `thejoker` is able to draw samples from the full posterior probability density function over orbital param-

eters and, despite the simplicity of the noise model (white noise) and single-companion assumption, it can be useful in characterizing the presence of massive planetary companions. `thejoker` uses a log-uniform prior for the period (between $0.4 < P < 410$ days), the Beta distribution (with $a = 0.867$ and $b = 3.03$) from Kipping (2013b) as a prior for the eccentricity, and a uniform prior for the argument of pericenter and the orbital phase. For the rejection sampling analysis, we ran $> \times 10^8$ (2^{27}) sam-

ples with `thejoker` exploring orbits with periods less than the RV baseline ($P < 410$ days).

A total of 2194159 samples survived ($\sim 1.63\%$ acceptance rate). We calculate the masses for the surviving samples assuming $\sin i = 1$ and place an upper limit (99th quantile) of $6.7M_J$ for companions with periods < 410 days (< 0.87 au). If we only permit circular orbits, the corresponding upper limit is $4.7M_J$. The HPF RVs suggest there are no low-inclination ($\sin i = 1$) Jupiter-mass gas giants within 0.87 AU of KOI-4777. These constraints from HPF RVs are a useful to probe the existence of additional non-transiting companions orbiting KOI-4777 because no additional transits were detected by the Kepler DR25 pipeline or [Caceres et al. \(2019a\)](#).

6.2. Bulk Composition of KOI-4777.01

KOI-4777.01 is on the extreme end of the USP population as it is the smallest validated planet in this population (Figure 7). Almost all validated and candidate USPs have radii $\lesssim 1.9R_\oplus$ and are expected to be largely rocky planets (e.g., [Sanchis-Ojeda et al. 2014](#); [Adams et al. 2021](#)). [Dai et al. \(2019\)](#) performed a homogeneous study of USP Earth-sized planets and found that USPs with $M_p < 8M_\oplus$ were consistent with having Earth-like compositions. While our upper mass limit from RVs is much larger than $8M_\oplus$, a more informative bound on the mass can be obtained by placing constraints on the bulk density. The minimum density for a USP can be approximated by requiring it to orbit outside the Roche limit (Equation 5 in [Rappaport et al. 2013](#)) to ensure that it is not destroyed by the host star’s tidal gravitational force. Following the assumption used by [Sanchis-Ojeda et al. \(2014\)](#), in which the USP’s core density is no more than twice its bulk density, the minimum density of KOI-4777.01 is $\rho_p \geq 1.31 \text{ g/cm}^3$, which corresponds to a minimum mass of $M_p \geq 0.025M_\oplus$. To derive an

upper density limit, the bulk density of KOI-4777 is required to be less than the density for the 100% iron model from [Zeng et al. \(2019\)](#).

Using our upper 3σ radius measurement, we constrain KOI-4777.01 to $M_p \leq 0.34M_\oplus$. If instead, we force the upper density limit to be that of an Earth-like rocky planet (32.5% iron-nickel alloy and 67.5% enstatite rock; [Zeng et al. 2019](#)), then KOI-4777.01 would have a mass $M_p \leq 0.18M_\oplus$. Both of these upper limits are larger than the mass of Mars ($0.1074 M_\oplus$).

Given the mass regime of $M_p \leq 0.34M_\oplus$, we expect KOI-4777.01 to be rocky and without a substantial volatile envelope. Figure 8 compares the calculated radius to known composition models to further investigate the bulk properties of KOI-4777.01. For comparison, we highlight published USPs contained in the NASA Exoplanet Archive and systems characterized with transit timing variations, such as the Kepler-444 Mars-sized planets ([Mills & Fabrycky 2017](#)), Kepler-138 b ([Almenara et al. 2018](#)), and the TRAPPIST-1 system ([Agol et al. 2021](#)). While the 1σ radius estimate of Kepler-138 b, Kepler-444 d, and Kepler-444 e all overlap with our 3σ radius measurement for KOI-4777.01, the aforementioned planets differ in the amount of insolation flux received. Kepler-138 b has a period of ~ 10.3 days and is found to be consistent with the presence of a thick volatile layer while the Kepler-444 planets have periods > 5 days and could not exclude composition models containing volatiles. KOI-4777.01 is inconsistent with non-rocky compositions with a substantial hydrogen, helium, or water atmosphere. No model from [Zeng et al. \(2019\)](#) with an atmospheric temperature 1000 K is within 3σ of our expected radius and this is consistent with simulations by [Lopez \(2017\)](#) which show that KOI-4777.01 is too irradiated ($F > 300F_\oplus$, $T_{eq} > 1000\text{K}$) and too small to hold onto any H/He envelope. A pure rocky or Earth-like composition passes through the mass and radius envelope (shaded

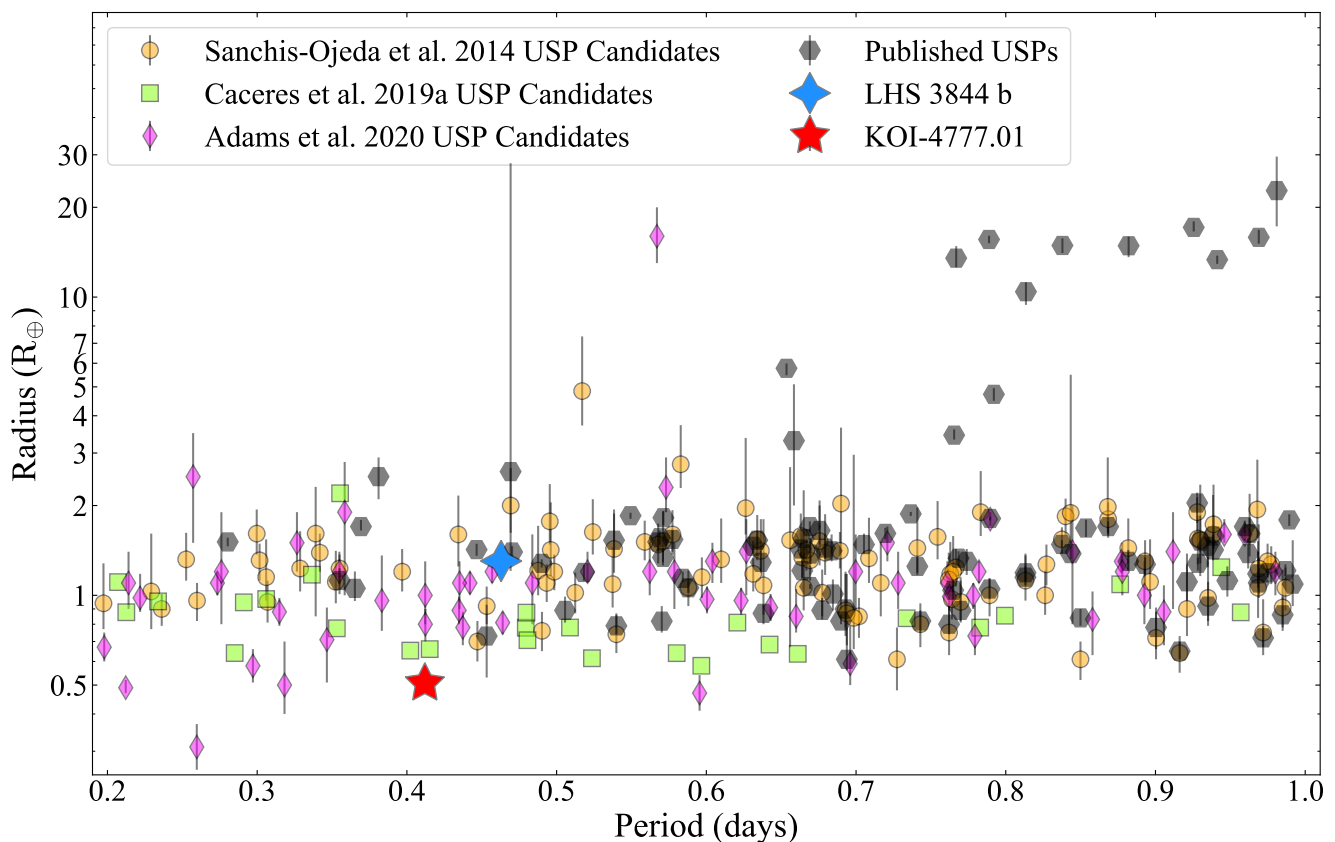


Figure 7. KOI-4777.01 compared in orbital period and planetary radius with other candidate USPs from Kepler (Sanchis-Ojeda et al. 2014; Caceres et al. 2019b) and K2 (Adams et al. 2021). USPs from literature were queried from the NASA Exoplanet Archive (Akeson et al. 2013) on 3 September 2021. LHS 3844 b (Vanderspek et al. 2019) is marked as the blue star and another USP orbiting a similar M dwarf. KOI-4777.01, with a radius of $0.51 \pm 0.03 R_{\oplus}$, is the smallest validated USP.

region in Figure 8) for KOI-4777.01. The recent analysis of well-characterized USPs by Dai et al. (2021) showed that USPs tend to be rocky and cluster around an Earth-like composition with iron core mass fractions of 0.32 ± 0.04 .

Planets acquire atmospheres either through direct nebular gas capture, planetesimal or cometary impacts, degassing during accretion, or volcanic outgassing (Elkins-Tanton & Seager 2008). Low-mass planets, like KOI-4777.01, cannot effectively capture enough primordial gas to build large initial envelopes. For present-day Earth and Mars ingassing from the stellar nebula is not considered to be the primary contributor to the mass of their atmospheres (e.g., Dauphas & Morbidelli 2013; Olson & Sharp 2019). Additional factors would

further limit the retention of a significant primary atmosphere, including stripping due to large impactors (Schlichting & Mukhopadhyay 2018) or hydrodynamic escape due to extreme UV and X-ray flux from a young stellar host (Sharp 2017). Work by Kite & Barnett (2020) suggests that secondary atmospheres on rocky planets near an M dwarf host are generally unfavorable when $T_e > 500$ K, in line with prior work describing the “cosmic shoreline” between planets with and without atmospheres (Zahnle & Catling 2017).

LHS 3844 b (Vanderspek et al. 2019) is comparable to KOI-4777.01. While it is larger than KOI-4777.01 with a radius of $\sim 1.3 R_{\oplus}$, LHS 3844 b is orbiting an M dwarf on a period of 11 hours and has a comparable equilibrium tem-

perature of 805 K. [Kreidberg et al. \(2019\)](#) observed LHS 3844 b with Spitzer and obtained a symmetric thermal phase curve with a large amplitude that was inconsistent with the presence of a thick atmosphere. The Spitzer thermal phase curve could be modeled assuming LHS 3844 b was a synchronously-rotating bare rock with a surface composition comparable to Mercury (largely basaltic). [Kane et al. \(2020\)](#) modeled LHS 3844 b and characterized it as a bare rock planet and suggested a volatile-poor composition. We also expect the rotational period of KOI-4777.01 to be synchronous with the orbital frequency because the timescale for spin synchronization is shorter than the timescale for circularization even if we adopt an extreme value for KOI-4777.01’s initial spin angular frequency ($\omega_p/n = 10^4$ in Equation 5 of [Bodenheimer et al. 2001](#)). As such, KOI-4777.01 may also exhibit stark contrasts between the day- and night-side temperatures if it does not possess an appreciable atmosphere.

It is also possible that KOI-4777.01 may have an atmosphere made up of high molecular weight species. Following accretion, impact rates decline and smaller impactors can instead contribute to the planet’s volatile inventory (e.g., [Genda & Abe 2005](#); [de Vries et al. 2016](#)). Likewise, the extreme UV decreases over longer timescales as the host star settles down (e.g., [Sanz-Forcada et al. 2011](#)). Together with the relatively slow escape of heavier atoms (e.g., [Gronoff et al. 2020](#)), this can produce secondary atmospheres for terrestrial planets dominated by H₂O and CO₂, much like those hypothesized for early Venus and Earth (e.g., [Hamano et al. 2013](#)). Alternatively, a long-lived magma ocean or substellar pond would permit rock vapor into the atmosphere, potentially contributing detectable quantities of Na, Fe, SiO, and Mg to the atmosphere, depending on the surface temperature (e.g., [Schaefer & Fegley 2009](#); [Costa et al. 2017](#)), although it is cooler than

other objects with evidence for such an atmosphere ([Frustagli et al. 2020](#)). KOI-4777.01 receives a high enough insolation flux that there could be surface melting even in the absence of an atmosphere ([Chao et al. 2021](#)), especially if the planet experiences tidal or inductive heating driven by its host star. The escape of these species from a magma ocean-derived atmosphere could result in a trailing comet-like tail and an asymmetric transit shape ([Bodman et al. 2018](#)). Given the magnitude of the transit depth itself (~ 121 ppm), however, the spectroscopic characterization of the planet’s atmosphere and inferences based on transit shape likely lies beyond the near-term capabilities of ground- and space-based observatories.

6.3. Prospects for Future Characterization

The faintness of the host star ($V = 16.4$, $J = 13.2$) and the small transit depth (~ 121 ppm) make additional photometric characterization of KOI-4777 difficult. Photometric observations from the ground are currently impossible given this small transit depth, and the precision required to detect a transit is beyond the capabilities of more recent space-based missions, such as TESS. No occultations of KOI-4777.01 are observed in the Kepler data, and this is not surprising as the eclipse depth is < 1 ppm in the Kepler bandpass.

A mass determination of KOI-4777 is also difficult. If we adopt the upper mass limit of $0.34M_{\oplus}$, we expect a semi-amplitude velocity of $K = 53$ cm/s which is beyond the reach of current instruments for such a faint target. The primary goal of additional RVs would be to further constrain the existence of long-period companions. KOI-4777 is an early M dwarf, and the RV information content for such stars (e.g., [Reiners et al. 2018](#)) is better matched to optical spectrographs with an extended red wavelength coverage, such as CARMENES [Quirrenbach et al. \(2014, 2018\)](#), MAROON-X ([Seifahrt et al. 2016](#)), or NEID ([Schwab et al. 2016](#)). Instru-

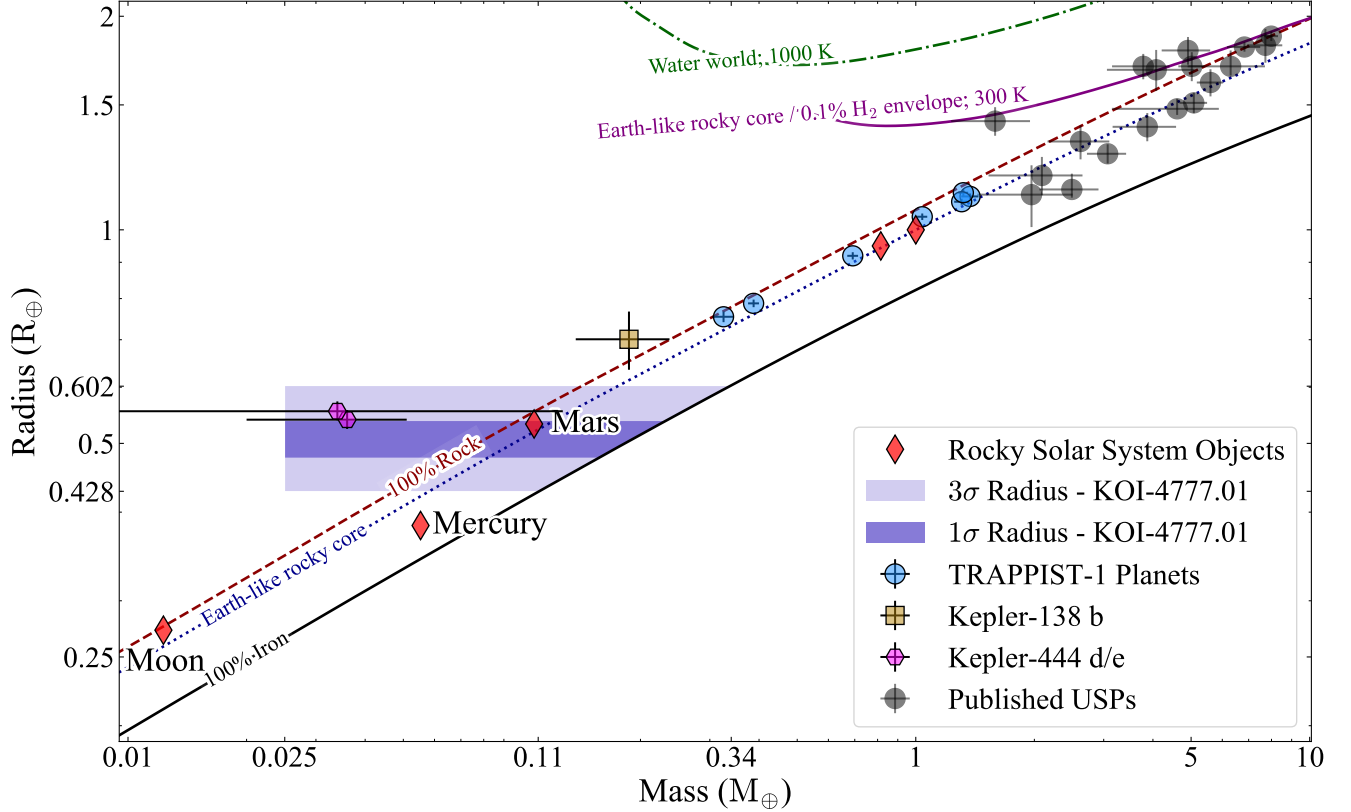


Figure 8. KOI-4777.01 on the mass-radius diagram. Without a mass measurement, we only constrain the most probable location of KOI-4777.01. The shaded regions indicate our 1σ and 3σ radius measurement, and incorporate limits on the mass from density constraints. For comparison, we include the inner Solar System planets and the Moon (red diamonds), well-characterized and small Kepler planets (Almenara et al. 2018; Mills & Fabrycky 2017), the TRAPPIST-1 system (Agol et al. 2021), and known USPs (gray points) from the NASA Exoplanet Archive (queried 3 September 2021). We include several model composition curves from Zeng et al. (2019). KOI-4777.01 is hot ($T_{eq} > 1000\text{K}$), and is incompatible with models that include an atmosphere with temperature effects. It is compatible with models of rocky planets with no significant volatile envelope.

ments with better precision can place tighter constraints on the existence of gas giants well beyond the ice-line for KOI-4777, and this is necessary to probe various formation scenarios.

7. SUMMARY

We have validated the planetary nature of the smallest known USP, a Mars-sized exoplanet transiting KOI-4777, an early M dwarf that was recovered from false positive status via manual vetting by the Kepler FPWG and independently identified by the ARPS analysis. Despite the prevalence of USPs in multi-planet systems, HPF RVs do not reveal the presence of any

low inclination ($\sin i = 1$) Jupiter-mass gas giant within 0.87 AU of KOI-4777. More precise RV observations could tighten these constraints. While additional ground and space-based characterization of KOI-4777.01 is beyond the precision capabilities of current photometric and RV instruments, we place limits on the mass using density limits. The span of masses and radii for KOI-4777.01 suggest it is most likely depleted of any extensive atmosphere.

ACKNOWLEDGMENTS

This work was supported by NASA Headquarters under the NASA Earth and Space

Science Fellowship Program through grant 80NSSC18K1114 and by the Alfred P. Sloan Foundation’s Minority Ph.D. Program through grant G-2016-20166039. The Center for Exoplanets and Habitable Worlds is supported by the Pennsylvania State University and the Eberly College of Science.

This is University of Texas Center for Planetary Systems Habitability Contribution #0038. These results are based on observations obtained with the Habitable-zone Planet Finder Spectrograph on the HET. We acknowledge support from NSF grants AST 1006676, AST 1126413, AST 1310875, AST 1310885, AST 2009889, AST 2108512 and the NASA Astrobiology Institute (NNA09DA76A) in our pursuit of precision radial velocities in the NIR. We acknowledge support from the Heising-Simons Foundation via grant 2017-0494. The Hobby-Eberly Telescope is a joint project of the University of Texas at Austin, the Pennsylvania State University, Ludwig-Maximilians-Universität München, and Georg-August Universität Göttingen. The HET is named in honor of its principal benefactors, William P. Hobby and Robert E. Eberly. The HET collaboration acknowledges the support and resources from the Texas Advanced Computing Center. We are grateful to the HET Resident Astronomers and Telescope Operators for their valuable assistance in gathering our HPF data. We are grateful to the HET Resident Astronomers and Telescope Operators for their valuable assistance in gathering our HPF data. We would like to acknowledge that the HET is built on Indigenous land. Moreover, we would like to acknowledge and pay our respects to the Carrizo & Comecrudo, Coahuiltecan, Caddo, Tonkawa, Comanche, Lipan Apache, Alabama-Coushatta, Kickapoo, Tigua Pueblo, and all the American Indian and Indigenous Peoples and communities who have been or have become a part of these

lands and territories in Texas, here on Turtle Island.

Computations for this research were performed on the Pennsylvania State University’s Institute for Computational and Data Sciences’ Roar supercomputer, including the CyberLAMP cluster supported by NSF grant MRI-1626251. The AutoRegressive Planet Search project at Penn State is supported by grants 80NSSC17K0122 from NASA and AST-1614690 from NSF.

Some of the data presented in this paper were obtained from from the Mikulski Archive for Space Telescopes (MAST) at the Space Telescope Science Institute. The specific observations analyzed can be accessed via [10.17909/t9-nqgs-a902](https://doi.org/10.17909/t9-nqgs-a902). Support for MAST for non-HST data is provided by the NASA Office of Space Science via grant NNX09AF08G and by other grants and contracts. This work includes data collected by the Kepler mission, which are publicly available from MAST. Funding for the Kepler mission is provided by the NASA Science Mission directorate.

This research made use of the NASA Exoplanet Archive, which is operated by Caltech, under contract with NASA under the Exoplanet Exploration Program. This research has made use of the SIMBAD database, operated at CDS, Strasbourg, France, and NASA’s Astrophysics Data System Bibliographic Services. 2MASS is a joint project of the University of Massachusetts and IPAC at Caltech, funded by NASA and the NSF.

The Digitized Sky Surveys were produced at STSci under U.S. Government grant NAG W-2166. The images of these surveys are based on photographic data obtained using the Oschin Schmidt Telescope on Palomar Mountain and the UK Schmidt Telescope. The plates were processed into the present compressed digital form with the permission of these institutions. The National Geographic Society - Palomar Ob-

servatory Sky Atlas (POSS-I) was made by the California Institute of Technology with grants from the National Geographic Society. The Oschin Schmidt Telescope is operated by the California Institute of Technology and Palomar Observatory.

This work has made use of data from the European Space Agency (ESA) mission *Gaia* (<https://www.cosmos.esa.int/gaia>), processed by the *Gaia* Data Processing and Analysis Consortium (DPAC, <https://www.cosmos.esa.int/web/gaia/dpac/consortium>). Funding for the DPAC has been provided by national institutions, in particular the institutions participating in the *Gaia* Multilateral Agreement.

Some observations were obtained from the Pan-STARRS1 Surveys (PS1). PS1 and the PS1 public science archive have been made possible through contributions by the Institute for Astronomy, the University of Hawaii, the Pan-STARRS Project Office, the Max-Planck Society and its participating institutes, the Max Planck Institute for Astronomy, Heidelberg and the Max Planck Institute for Extraterrestrial Physics, Garching, The Johns Hopkins University, Durham University, the University of Edinburgh, the Queen's University Belfast, the

Harvard-Smithsonian Center for Astrophysics, the Las Cumbres Observatory Global Telescope Network Incorporated, the National Central University of Taiwan, the Space Telescope Science Institute, the National Aeronautics and Space Administration under Grant No. NNX08AR22G issued through the Planetary Science Division of the NASA Science Mission Directorate, the National Science Foundation Grant No. AST-1238877, the University of Maryland, Eotvos Lorand University (ELTE), the Los Alamos National Laboratory, and the Gordon and Betty Moore Foundation.

Facilities: Gaia, HET (HPF), KPNO:2.1m (Robo-AO), PS1, Kepler

Software: ARC2 (Aigrain et al. 2017), *astroquery* (Ginsburg et al. 2019), *astropy* (Astropy Collaboration et al. 2018), *barycorrpy* (Kanodia & Wright 2018), *batman* (Kreidberg 2015), *dynesty* (Speagle 2020), EXOFASTv2 (Eastman et al. 2019), *galpy* (Bovy 2015), HPF-SpecMatch, *juliet* (Espinoza et al. 2019), *matplotlib* (Hunter 2007), *numpy* (van der Walt et al. 2011), *pandas* (McKinney 2010), *radvel* (Fulton et al. 2018), *scipy* (Virtanen et al. 2020), *SERVAL*, *telfit* (Gullikson et al. 2014), *VESPA* (Morton 2012)

REFERENCES

- Adams, E. R., Jackson, B., Endl, M., et al. 2017, *AJ*, 153, 82, doi: [10.3847/1538-3881/153/2/82](https://doi.org/10.3847/1538-3881/153/2/82)
- Adams, E. R., Jackson, B., Johnson, S., et al. 2021, *PSJ*, 2, 152, doi: [10.3847/PSJ/ac0ea0](https://doi.org/10.3847/PSJ/ac0ea0)
- Agol, E., Dorn, C., Grimm, S. L., et al. 2021, *The Planetary Science Journal*, 2, 1, doi: [10.3847/PSJ/abd022](https://doi.org/10.3847/PSJ/abd022)
- Aigrain, S., Parviainen, H., Roberts, S., Reece, S., & Evans, T. 2017, *MNRAS*, 471, 759, doi: [10.1093/mnras/stx1422](https://doi.org/10.1093/mnras/stx1422)
- Akeson, R. L., Chen, X., Ciardi, D., et al. 2013, *PASP*, 125, 989, doi: [10.1086/672273](https://doi.org/10.1086/672273)
- Almenara, J. M., Díaz, R. F., Dorn, C., Bonfils, X., & Udry, S. 2018, *MNRAS*, 478, 460, doi: [10.1093/mnras/sty1050](https://doi.org/10.1093/mnras/sty1050)
- Anglada-Escudé, G., & Butler, R. P. 2012, *ApJS*, 200, 15, doi: [10.1088/0067-0049/200/2/15](https://doi.org/10.1088/0067-0049/200/2/15)
- Angus, R., Morton, T., Aigrain, S., Foreman-Mackey, D., & Rajpaul, V. 2018, *MNRAS*, 474, 2094, doi: [10.1093/mnras/stx2109](https://doi.org/10.1093/mnras/stx2109)
- Astropy Collaboration, Price-Whelan, A. M., Sipőcz, B. M., et al. 2018, *AJ*, 156, 123, doi: [10.3847/1538-3881/aabc4f](https://doi.org/10.3847/1538-3881/aabc4f)
- Bailer-Jones, C. A. L., Rybizki, J., Foesneau, M., Demleitner, M., & Andrae, R. 2021, *AJ*, 161, 147, doi: [10.3847/1538-3881/abd806](https://doi.org/10.3847/1538-3881/abd806)
- Baranec, C., Riddle, R., Law, N. M., et al. 2013, *Journal of Vibration Engineering*, 72, 50021, doi: [10.3791/50021](https://doi.org/10.3791/50021)

- . 2014, *ApJL*, 790, L8,
doi: [10.1088/2041-8205/790/1/L8](https://doi.org/10.1088/2041-8205/790/1/L8)
- Bensby, T., Feltzing, S., & Oey, M. S. 2014, *A&A*, 562, A71, doi: [10.1051/0004-6361/201322631](https://doi.org/10.1051/0004-6361/201322631)
- Bluhm, P., Pallé, E., Molaverdikhani, K., et al. 2021, *A&A*, 650, A78,
doi: [10.1051/0004-6361/202140688](https://doi.org/10.1051/0004-6361/202140688)
- Bodenheimer, P., Lin, D. N. C., & Mardling, R. A. 2001, *ApJ*, 548, 466, doi: [10.1086/318667](https://doi.org/10.1086/318667)
- Bodman, E. H. L., Wright, J. T., Desch, S. J., & Lisse, C. M. 2018, *AJ*, 156, 173,
doi: [10.3847/1538-3881/aadc60](https://doi.org/10.3847/1538-3881/aadc60)
- Borucki, W. J., Koch, D., Basri, G., et al. 2010, *Science*, 327, 977, doi: [10.1126/science.1185402](https://doi.org/10.1126/science.1185402)
- Bovy, J. 2015, *ApJS*, 216, 29,
doi: [10.1088/0067-0049/216/2/29](https://doi.org/10.1088/0067-0049/216/2/29)
- Bravo, J. P., Roque, S., Estrela, R., Leão, I. C., & De Medeiros, J. R. 2014, *A&A*, 568, A34,
doi: [10.1051/0004-6361/201323032](https://doi.org/10.1051/0004-6361/201323032)
- Brown, T. M., Latham, D. W., Everett, M. E., & Esquerdo, G. A. 2011, *AJ*, 142, 112,
doi: [10.1088/0004-6256/142/4/112](https://doi.org/10.1088/0004-6256/142/4/112)
- Caceres, G. A., Feigelson, E. D., Jogesh Babu, G., et al. 2019a, *AJ*, 158, 58,
doi: [10.3847/1538-3881/ab26ba](https://doi.org/10.3847/1538-3881/ab26ba)
- . 2019b, *AJ*, 158, 57,
doi: [10.3847/1538-3881/ab26b8](https://doi.org/10.3847/1538-3881/ab26b8)
- Canto Martins, B. L., Gomes, R. L., Messias, Y. S., et al. 2020, *ApJS*, 250, 20,
doi: [10.3847/1538-4365/aba73f](https://doi.org/10.3847/1538-4365/aba73f)
- Chambers, K. C., Magnier, E. A., Metcalfe, N., et al. 2016, arXiv e-prints, arXiv:1612.05560.
<https://arxiv.org/abs/1612.05560>
- Chao, K.-H., deGraffenried, R., Lach, M., et al. 2021, *Chemie der Erde / Geochemistry*, 81, 125735, doi: [10.1016/j.chemer.2020.125735](https://doi.org/10.1016/j.chemer.2020.125735)
- Choi, J., Dotter, A., Conroy, C., et al. 2016, *ApJ*, 823, 102, doi: [10.3847/0004-637X/823/2/102](https://doi.org/10.3847/0004-637X/823/2/102)
- Clough, S. A., Shephard, M. W., Mlawer, E. J., et al. 2005, *JQSRT*, 91, 233,
doi: [10.1016/j.jqsrt.2004.05.058](https://doi.org/10.1016/j.jqsrt.2004.05.058)
- Cloutier, R., Eastman, J. D., Rodriguez, J. E., et al. 2020, *AJ*, 160, 3,
doi: [10.3847/1538-3881/ab91c2](https://doi.org/10.3847/1538-3881/ab91c2)
- Cloutier, R., Charbonneau, D., Stassun, K. G., et al. 2021, *AJ*, 162, 79,
doi: [10.3847/1538-3881/ac0157](https://doi.org/10.3847/1538-3881/ac0157)
- Costa, G. C. C., Jacobson, N. S., & Fegley, Bruce, J. 2017, *Icarus*, 289, 42,
doi: [10.1016/j.icarus.2017.02.006](https://doi.org/10.1016/j.icarus.2017.02.006)
- Coughlin, J. 2019, in *American Astronomical Society Meeting Abstracts*, Vol. 51, American Astronomical Society Meeting Abstracts #234, 113.01
- Coughlin, J. L., Mullally, F., Thompson, S. E., et al. 2016, *ApJS*, 224, 12,
doi: [10.3847/0067-0049/224/1/12](https://doi.org/10.3847/0067-0049/224/1/12)
- Crossfield, I. J. M., Waalkes, W., Newton, E. R., et al. 2019, *ApJL*, 883, L16,
doi: [10.3847/2041-8213/ab3d30](https://doi.org/10.3847/2041-8213/ab3d30)
- Cui, K., Liu, J., Yang, S., et al. 2019, *MNRAS*, 489, 5513, doi: [10.1093/mnras/stz2432](https://doi.org/10.1093/mnras/stz2432)
- Cutri, R. M., Skrutskie, M. F., van Dyk, S., et al. 2003, *VizieR Online Data Catalog*, 2246
- Dai, F., Masuda, K., & Winn, J. N. 2018, *ApJL*, 864, L38, doi: [10.3847/2041-8213/aadd4f](https://doi.org/10.3847/2041-8213/aadd4f)
- Dai, F., Masuda, K., Winn, J. N., & Zeng, L. 2019, *ApJ*, 883, 79, doi: [10.3847/1538-4357/ab3a3b](https://doi.org/10.3847/1538-4357/ab3a3b)
- Dai, F., Howard, A. W., Batalha, N. M., et al. 2021, arXiv e-prints, arXiv:2105.08844.
<https://arxiv.org/abs/2105.08844>
- Dauphas, N., & Morbidelli, A. 2013, arXiv e-prints, arXiv:1312.1202.
<https://arxiv.org/abs/1312.1202>
- de Vries, J., Nimmo, F., Melosh, H. J., et al. 2016, *Progress in Earth and Planetary Science*, 3, 7,
doi: [10.1186/s40645-016-0083-8](https://doi.org/10.1186/s40645-016-0083-8)
- Dotter, A. 2016, *ApJS*, 222, 8,
doi: [10.3847/0067-0049/222/1/8](https://doi.org/10.3847/0067-0049/222/1/8)
- Eastman, J. D., Rodriguez, J. E., Agol, E., et al. 2019, arXiv e-prints, arXiv:1907.09480.
<https://arxiv.org/abs/1907.09480>
- Eggleton, P. P. 1983, *ApJ*, 268, 368,
doi: [10.1086/160960](https://doi.org/10.1086/160960)
- Elkins-Tanton, L. T., & Seager, S. 2008, *ApJ*, 685, 1237, doi: [10.1086/591433](https://doi.org/10.1086/591433)
- Espinoza, N., Kossakowski, D., & Brahm, R. 2019, *MNRAS*, 490, 2262, doi: [10.1093/mnras/stz2688](https://doi.org/10.1093/mnras/stz2688)
- Everett, M. E., Howell, S. B., & Kinemuchi, K. 2012, *PASP*, 124, 316, doi: [10.1086/665529](https://doi.org/10.1086/665529)
- Fitzpatrick, E. L. 1999, *PASP*, 111, 63,
doi: [10.1086/316293](https://doi.org/10.1086/316293)
- Foreman-Mackey, D., Agol, E., Ambikasaran, S., & Angus, R. 2017, *AJ*, 154, 220,
doi: [10.3847/1538-3881/aa9332](https://doi.org/10.3847/1538-3881/aa9332)
- Frustagli, G., Poretti, E., Milbourne, T., et al. 2020, *A&A*, 633, A133,
doi: [10.1051/0004-6361/201936689](https://doi.org/10.1051/0004-6361/201936689)

- Fulton, B. J., Petigura, E. A., Blunt, S., & Sinukoff, E. 2018, *PASP*, 130, 044504, doi: [10.1088/1538-3873/aaaaa8](https://doi.org/10.1088/1538-3873/aaaaa8)
- Gagné, J., Mamajek, E. E., Malo, L., et al. 2018, *ApJ*, 856, 23, doi: [10.3847/1538-4357/aaae09](https://doi.org/10.3847/1538-4357/aaae09)
- Gaia Collaboration, Brown, A. G. A., Vallenari, A., et al. 2021, *A&A*, 649, A1, doi: [10.1051/0004-6361/202039657](https://doi.org/10.1051/0004-6361/202039657)
- Genda, H., & Abe, Y. 2005, *Nature*, 433, 842, doi: [10.1038/nature03360](https://doi.org/10.1038/nature03360)
- Gilliland, R. L., Chaplin, W. J., Jenkins, J. M., Ramsey, L. W., & Smith, J. C. 2015, *AJ*, 150, 133, doi: [10.1088/0004-6256/150/4/133](https://doi.org/10.1088/0004-6256/150/4/133)
- Ginsburg, A., Sipőcz, B. M., Brasseur, C. E., et al. 2019, *AJ*, 157, 98, doi: [10.3847/1538-3881/aafc33](https://doi.org/10.3847/1538-3881/aafc33)
- Goldreich, P., & Soter, S. 1966, *Icarus*, 5, 375, doi: [10.1016/0019-1035\(66\)90051-0](https://doi.org/10.1016/0019-1035(66)90051-0)
- Green, G. M., Schlafly, E., Zucker, C., Speagle, J. S., & Finkbeiner, D. 2019, *ApJ*, 887, 93, doi: [10.3847/1538-4357/ab5362](https://doi.org/10.3847/1538-4357/ab5362)
- Gronoff, G., Arras, P., Baraka, S., et al. 2020, *Journal of Geophysical Research (Space Physics)*, 125, e27639, doi: [10.1029/2019JA027639](https://doi.org/10.1029/2019JA027639)
- Gullikson, K., Dodson-Robinson, S., & Kraus, A. 2014, *AJ*, 148, 53, doi: [10.1088/0004-6256/148/3/53](https://doi.org/10.1088/0004-6256/148/3/53)
- Hamano, K., Abe, Y., & Genda, H. 2013, *Nature*, 497, 607, doi: [10.1038/nature12163](https://doi.org/10.1038/nature12163)
- Hamer, J. H., & Schlafman, K. C. 2020, *AJ*, 160, 138, doi: [10.3847/1538-3881/aba74f](https://doi.org/10.3847/1538-3881/aba74f)
- Hirano, T., Dai, F., Gandolfi, D., et al. 2018, *AJ*, 155, 127, doi: [10.3847/1538-3881/aaa9c1](https://doi.org/10.3847/1538-3881/aaa9c1)
- Hirano, T., Livingston, J. H., Fukui, A., et al. 2021, *AJ*, 162, 161, doi: [10.3847/1538-3881/ac0fdc](https://doi.org/10.3847/1538-3881/ac0fdc)
- Howell, S. B., Sobek, C., Haas, M., et al. 2014, *PASP*, 126, 398, doi: [10.1086/676406](https://doi.org/10.1086/676406)
- Hunter, J. D. 2007, *Computing In Science & Engineering*, 9, 90, doi: [10.1109/MCSE.2007.55](https://doi.org/10.1109/MCSE.2007.55)
- Irwin, J., Berta, Z. K., Burke, C. J., et al. 2011, *ApJ*, 727, 56, doi: [10.1088/0004-637X/727/1/56](https://doi.org/10.1088/0004-637X/727/1/56)
- Jackson, B., Barnes, R., & Greenberg, R. 2008a, *MNRAS*, 391, 237, doi: [10.1111/j.1365-2966.2008.13868.x](https://doi.org/10.1111/j.1365-2966.2008.13868.x)
- Jackson, B., Greenberg, R., & Barnes, R. 2008b, *ApJ*, 678, 1396, doi: [10.1086/529187](https://doi.org/10.1086/529187)
- Jensen-Clem, R., Duev, D. A., Riddle, R., et al. 2018, *AJ*, 155, 32, doi: [10.3847/1538-3881/aa9be6](https://doi.org/10.3847/1538-3881/aa9be6)
- Johnson, D. R. H., & Soderblom, D. R. 1987, *AJ*, 93, 864, doi: [10.1086/114370](https://doi.org/10.1086/114370)
- Kane, S. R., Roettenbacher, R. M., Unterborn, C. T., Foley, B. J., & Hill, M. L. 2020, *The Planetary Science Journal*, 1, 36, doi: [10.3847/PSJ/abaab5](https://doi.org/10.3847/PSJ/abaab5)
- Kanodia, S., & Wright, J. 2018, *Research Notes of the American Astronomical Society*, 2, 4, doi: [10.3847/2515-5172/aaa4b7](https://doi.org/10.3847/2515-5172/aaa4b7)
- Kaplan, K. F., Bender, C. F., Terrien, R. C., et al. 2019, in *Astronomical Society of the Pacific Conference Series*, Vol. 523, *Astronomical Data Analysis Software and Systems XXVII*, ed. P. J. Teuben, M. W. Pound, B. A. Thomas, & E. M. Warner, 567
- Kinemuchi, K., Barclay, T., Fanelli, M., et al. 2012, *PASP*, 124, 963, doi: [10.1086/667603](https://doi.org/10.1086/667603)
- Kipping, D. M. 2013a, *MNRAS*, 435, 2152, doi: [10.1093/mnras/stt1435](https://doi.org/10.1093/mnras/stt1435)
- . 2013b, *MNRAS*, 434, L51, doi: [10.1093/mnras/slt075](https://doi.org/10.1093/mnras/slt075)
- Kite, E. S., & Barnett, M. N. 2020, *Proceedings of the National Academy of Science*, 117, 18264, <https://arxiv.org/abs/2006.02589>
- Kreidberg, L. 2015, *batman: BAsic Transit Model cAlculationN in Python*, *Astrophysics Source Code Library*. <http://ascl.net/1510.002>
- Kreidberg, L., Koll, D. D. B., Morley, C., et al. 2019, *Nature*, 573, 87, doi: [10.1038/s41586-019-1497-4](https://doi.org/10.1038/s41586-019-1497-4)
- Kurucz, R. L. 1970, *SAO Special Report*, 309
- . 1993, *SYNTHE spectrum synthesis programs and line data*
- Lee, E. J., & Chiang, E. 2017, *ApJ*, 842, 40, doi: [10.3847/1538-4357/aa6fb3](https://doi.org/10.3847/1538-4357/aa6fb3)
- Lopez, E. D. 2017, *MNRAS*, 472, 245, doi: [10.1093/mnras/stx1558](https://doi.org/10.1093/mnras/stx1558)
- Magnier, E. A., Schlafly, E. F., Finkbeiner, D. P., et al. 2020, *ApJS*, 251, 6, doi: [10.3847/1538-4365/abb82a](https://doi.org/10.3847/1538-4365/abb82a)
- Mahadevan, S., Ramsey, L., Bender, C., et al. 2012, in *Society of Photo-Optical Instrumentation Engineers (SPIE) Conference Series*, Vol. 8446, *Proc. SPIE*, 84461S, doi: [10.1117/12.926102](https://doi.org/10.1117/12.926102)

- Mahadevan, S., Ramsey, L. W., Terrien, R., et al. 2014, in Proc. SPIE, Vol. 9147, Ground-based and Airborne Instrumentation for Astronomy V, 91471G, doi: [10.1117/12.2056417](https://doi.org/10.1117/12.2056417)
- McKinney, W. 2010, in Proceedings of the 9th Python in Science Conference, ed. S. van der Walt & J. Millman, 51 – 56
- McQuillan, A., Aigrain, S., & Mazeh, T. 2013a, MNRAS, 432, 1203, doi: [10.1093/mnras/stt536](https://doi.org/10.1093/mnras/stt536)
- McQuillan, A., Mazeh, T., & Aigrain, S. 2013b, ApJL, 775, L11, doi: [10.1088/2041-8205/775/1/L11](https://doi.org/10.1088/2041-8205/775/1/L11)
- Metcalfe, A., Anderson, T., Bender, C., et al. 2019, Optica, 6, 233, doi: [10.1364/OPTICA.6.000233](https://doi.org/10.1364/OPTICA.6.000233)
- Millholland, S. C., & Spalding, C. 2020, ApJ, 905, 71, doi: [10.3847/1538-4357/abc4e5](https://doi.org/10.3847/1538-4357/abc4e5)
- Mills, S. M., & Fabrycky, D. C. 2017, ApJL, 838, L11, doi: [10.3847/2041-8213/aa6543](https://doi.org/10.3847/2041-8213/aa6543)
- Minkowski, R. L., & Abell, G. O. 1963, The National Geographic Society-Palomar Observatory Sky Survey, ed. K. A. Strand, 481
- Morton, T. D. 2012, ApJ, 761, 6, doi: [10.1088/0004-637X/761/1/6](https://doi.org/10.1088/0004-637X/761/1/6)
- . 2015, isochrones: Stellar model grid package, Astrophysics Source Code Library. <http://ascl.net/1503.010>
- Morton, T. D., Bryson, S. T., Coughlin, J. L., et al. 2016, ApJ, 822, 86, doi: [10.3847/0004-637X/822/2/86](https://doi.org/10.3847/0004-637X/822/2/86)
- Muirhead, P. S., Johnson, J. A., Apps, K., et al. 2012, ApJ, 747, 144, doi: [10.1088/0004-637X/747/2/144](https://doi.org/10.1088/0004-637X/747/2/144)
- Mullally, F., Coughlin, J. L., Thompson, S. E., et al. 2016, PASP, 128, 074502, doi: [10.1088/1538-3873/128/965/074502](https://doi.org/10.1088/1538-3873/128/965/074502)
- Newton, E. R., Irwin, J., Charbonneau, D., et al. 2016, ApJ, 821, 93, doi: [10.3847/0004-637X/821/2/93](https://doi.org/10.3847/0004-637X/821/2/93)
- Ninan, J. P., Bender, C. F., Mahadevan, S., et al. 2018, in Society of Photo-Optical Instrumentation Engineers (SPIE) Conference Series, Vol. 10709, Proc. SPIE, 107092U, doi: [10.1117/12.2312787](https://doi.org/10.1117/12.2312787)
- Nowak, G., Luque, R., Parviainen, H., et al. 2020, A&A, 642, A173, doi: [10.1051/0004-6361/202037867](https://doi.org/10.1051/0004-6361/202037867)
- Olson, P. L., & Sharp, Z. D. 2019, Physics of the Earth and Planetary Interiors, 294, 106294, doi: [10.1016/j.pepi.2019.106294](https://doi.org/10.1016/j.pepi.2019.106294)
- Petrovich, C., Deibert, E., & Wu, Y. 2019, AJ, 157, 180, doi: [10.3847/1538-3881/ab0e0a](https://doi.org/10.3847/1538-3881/ab0e0a)
- Price-Whelan, A. M., Hogg, D. W., Foreman-Mackey, D., & Rix, H.-W. 2017, ApJ, 837, 20, doi: [10.3847/1538-4357/aa5e50](https://doi.org/10.3847/1538-4357/aa5e50)
- Pu, B., & Lai, D. 2019, MNRAS, 488, 3568, doi: [10.1093/mnras/stz1817](https://doi.org/10.1093/mnras/stz1817)
- Quirrenbach, A., Amado, P. J., Caballero, J. A., et al. 2014, in Society of Photo-Optical Instrumentation Engineers (SPIE) Conference Series, Vol. 9147, Proc. SPIE, 91471F, doi: [10.1117/12.2056453](https://doi.org/10.1117/12.2056453)
- Quirrenbach, A., Amado, P. J., Ribas, I., et al. 2018, in Society of Photo-Optical Instrumentation Engineers (SPIE) Conference Series, Vol. 10702, Proc. SPIE, 107020W, doi: [10.1117/12.2313689](https://doi.org/10.1117/12.2313689)
- Rappaport, S., Sanchis-Ojeda, R., Rogers, L. A., Levine, A., & Winn, J. N. 2013, ApJL, 773, L15, doi: [10.1088/2041-8205/773/1/L15](https://doi.org/10.1088/2041-8205/773/1/L15)
- Reiners, A., Zechmeister, M., Caballero, J. A., et al. 2018, A&A, 612, A49, doi: [10.1051/0004-6361/201732054](https://doi.org/10.1051/0004-6361/201732054)
- Reinhold, T., & Hekker, S. 2020, A&A, 635, A43, doi: [10.1051/0004-6361/201936887](https://doi.org/10.1051/0004-6361/201936887)
- Ricker, G. R., Winn, J. N., Vanderspek, R., et al. 2015, Journal of Astronomical Telescopes, Instruments, and Systems, 1, 014003, doi: [10.1117/1.JATIS.1.1.014003](https://doi.org/10.1117/1.JATIS.1.1.014003)
- Sanchis-Ojeda, R., Rappaport, S., Winn, J. N., et al. 2014, ApJ, 787, 47, doi: [10.1088/0004-637X/787/1/47](https://doi.org/10.1088/0004-637X/787/1/47)
- Sanchis-Ojeda, R., Rappaport, S., Pallè, E., et al. 2015, ApJ, 812, 112, doi: [10.1088/0004-637X/812/2/112](https://doi.org/10.1088/0004-637X/812/2/112)
- Sanz-Forcada, J., Micela, G., Ribas, I., et al. 2011, A&A, 532, A6, doi: [10.1051/0004-6361/201116594](https://doi.org/10.1051/0004-6361/201116594)
- Schaefer, L., & Fegley, B. 2009, ApJL, 703, L113, doi: [10.1088/0004-637X/703/2/L113](https://doi.org/10.1088/0004-637X/703/2/L113)
- Schlaufman, K. C., Lin, D. N. C., & Ida, S. 2010, ApJL, 724, L53, doi: [10.1088/2041-8205/724/1/L53](https://doi.org/10.1088/2041-8205/724/1/L53)
- Schlichting, H. E., & Mukhopadhyay, S. 2018, SSRv, 214, 34, doi: [10.1007/s11214-018-0471-z](https://doi.org/10.1007/s11214-018-0471-z)
- Schönrich, R., Binney, J., & Dehnen, W. 2010, MNRAS, 403, 1829, doi: [10.1111/j.1365-2966.2010.16253.x](https://doi.org/10.1111/j.1365-2966.2010.16253.x)

- Schwab, C., Rakich, A., Gong, Q., et al. 2016, Society of Photo-Optical Instrumentation Engineers (SPIE) Conference Series, Vol. 9908, Design of NEID, an extreme precision Doppler spectrograph for WIYN, 99087H, doi: [10.1117/12.2234411](https://doi.org/10.1117/12.2234411)
- Seifahrt, A., Bean, J. L., Stürmer, J., et al. 2016, in Society of Photo-Optical Instrumentation Engineers (SPIE) Conference Series, Vol. 9908, Ground-based and Airborne Instrumentation for Astronomy VI, ed. C. J. Evans, L. Simard, & H. Takami, 990818, doi: [10.1117/12.2232069](https://doi.org/10.1117/12.2232069)
- Sharp, Z. D. 2017, *Chemical Geology*, 448, 137, doi: [10.1016/j.chemgeo.2016.11.018](https://doi.org/10.1016/j.chemgeo.2016.11.018)
- Shetrone, M., Cornell, M. E., Fowler, J. R., et al. 2007, *PASP*, 119, 556, doi: [10.1086/519291](https://doi.org/10.1086/519291)
- Shporer, A., Collins, K. A., Astudillo-Defru, N., et al. 2020, *ApJL*, 890, L7, doi: [10.3847/2041-8213/ab7020](https://doi.org/10.3847/2041-8213/ab7020)
- Smith, A. M. S., Cabrera, J., Csizmadia, S., et al. 2018, *MNRAS*, 474, 5523, doi: [10.1093/mnras/stx2891](https://doi.org/10.1093/mnras/stx2891)
- Smith, J. C., Stumpe, M. C., Van Cleve, J. E., et al. 2012, *PASP*, 124, 1000, doi: [10.1086/667697](https://doi.org/10.1086/667697)
- Speagle, J. S. 2020, *MNRAS*, 493, 3132, doi: [10.1093/mnras/staa278](https://doi.org/10.1093/mnras/staa278)
- Stefánsson, G., Hearty, F., Robertson, P., et al. 2016, *ApJ*, 833, 175, doi: [10.3847/1538-4357/833/2/175](https://doi.org/10.3847/1538-4357/833/2/175)
- Stefánsson, G., Cañas, C., Wisniewski, J., et al. 2020, *AJ*, 159, 100, doi: [10.3847/1538-3881/ab5f15](https://doi.org/10.3847/1538-3881/ab5f15)
- Stefánsson, G., Mahadevan, S., Maney, M., et al. 2020, *AJ*, 160, 192, doi: [10.3847/1538-3881/abb13a](https://doi.org/10.3847/1538-3881/abb13a)
- Steffen, J. H., & Farr, W. M. 2013, *ApJL*, 774, L12, doi: [10.1088/2041-8205/774/1/L12](https://doi.org/10.1088/2041-8205/774/1/L12)
- Stumpe, M. C., Smith, J. C., Van Cleve, J. E., et al. 2012, *PASP*, 124, 985, doi: [10.1086/667698](https://doi.org/10.1086/667698)
- Swift, J. J., Johnson, J. A., Morton, T. D., et al. 2013, *ApJ*, 764, 105, doi: [10.1088/0004-637X/764/1/105](https://doi.org/10.1088/0004-637X/764/1/105)
- Thompson, S. E., Fraquelli, D., Van Cleve, J. E., & Caldwell, D. A. 2016, Kepler Archive Manual, Kepler Science Document KDMC-10008-006
- Thompson, S. E., Coughlin, J. L., Hoffman, K., et al. 2018, *ApJS*, 235, 38, doi: [10.3847/1538-4365/aab4f9](https://doi.org/10.3847/1538-4365/aab4f9)
- Twicken, J. D., Jenkins, J. M., Seader, S. E., et al. 2016, *AJ*, 152, 158, doi: [10.3847/0004-6256/152/6/158](https://doi.org/10.3847/0004-6256/152/6/158)
- Van Cleve, J. E., Christiansen, J. L., Jenkins, J. M., et al. 2016, Kepler Data Characteristics Handbook, Kepler Science Document KSCI-19040-005
- van der Walt, S., Colbert, S. C., & Varoquaux, G. 2011, *Computing in Science and Engineering*, 13, 22, doi: [10.1109/MCSE.2011.37](https://doi.org/10.1109/MCSE.2011.37)
- Vanderspek, R., Huang, C. X., Vanderburg, A., et al. 2019, *ApJL*, 871, L24, doi: [10.3847/2041-8213/aafb7a](https://doi.org/10.3847/2041-8213/aafb7a)
- Virtanen, P., Gommers, R., Oliphant, T. E., et al. 2020, *Nature Methods*, 17, 261, doi: [10.1038/s41592-019-0686-2](https://doi.org/10.1038/s41592-019-0686-2)
- Winn, J. N., Sanchis-Ojeda, R., & Rappaport, S. 2018, *NewAR*, 83, 37, doi: [10.1016/j.newar.2019.03.006](https://doi.org/10.1016/j.newar.2019.03.006)
- Worthey, G. 1994, *ApJS*, 95, 107, doi: [10.1086/192096](https://doi.org/10.1086/192096)
- Wright, E. L., Eisenhardt, P. R. M., Mainzer, A. K., et al. 2010, *AJ*, 140, 1868, doi: [10.1088/0004-6256/140/6/1868](https://doi.org/10.1088/0004-6256/140/6/1868)
- Wright, J. T., & Eastman, J. D. 2014, *PASP*, 126, 838, doi: [10.1086/678541](https://doi.org/10.1086/678541)
- Yee, S. W., Petigura, E. A., & von Braun, K. 2017, *ApJ*, 836, 77, doi: [10.3847/1538-4357/836/1/77](https://doi.org/10.3847/1538-4357/836/1/77)
- Zahnle, K. J., & Catling, D. C. 2017, *ApJ*, 843, 122, doi: [10.3847/1538-4357/aa7846](https://doi.org/10.3847/1538-4357/aa7846)
- Zawadzki, B., Carrera, D., & Ford, E. B. 2021, *MNRAS*, 503, 1390, doi: [10.1093/mnras/stab603](https://doi.org/10.1093/mnras/stab603)
- Zechmeister, M., & Kürster, M. 2009, *A&A*, 496, 577, doi: [10.1051/0004-6361:200811296](https://doi.org/10.1051/0004-6361:200811296)
- Zechmeister, M., Reiners, A., Amado, P. J., et al. 2018, *A&A*, 609, A12, doi: [10.1051/0004-6361/201731483](https://doi.org/10.1051/0004-6361/201731483)
- Zeng, L., Jacobsen, S. B., Sasselov, D. D., et al. 2019, *Proceedings of the National Academy of Science*, 116, 9723, doi: [10.1073/pnas.1812905116](https://doi.org/10.1073/pnas.1812905116)
- Ziegler, C., Law, N. M., Baranec, C., et al. 2018, *AJ*, 155, 161, doi: [10.3847/1538-3881/aab042](https://doi.org/10.3847/1538-3881/aab042)